2024

Wave Energy Converter Wave Force Prediction Using a Neural Network

Morgan Kline
Michigan Technological University, mkline@mtu.edu

WAVE ENERGY CONVERTER WAVE FORCE PREDICTION USING A NEURAL NETWORK

By

Morgan Kline

A THESIS

Submitted in partial fulfillment of the requirements for the degree of

MASTER OF SCIENCE

In Mechanical Engineering

MICHIGAN TECHNOLOGICAL UNIVERSITY

2024

This thesis has been approved in partial fulfillment of the requirements for the Degree of MASTER OF SCIENCE in Mechanical Engineering.

Department of Mechanical Engineering - Engineering Mechanics

Thesis Advisor: *Dr. Gordon Parker*

Committee Member: *Dr. Jungyun Bae*

Committee Member: *Dr. William Endres*

Department Chair: *Dr. Jason Blough*

Contents

List of Figures

List of Tables

Acknowledgments

This work has been made possible thanks to the unwaivering support of my advisor, Dr. Gordon Parker. His committment to the the success of this project, and the growth of his students, both as individuals and engineers is unsurpassed. It is largely because of his time, effort, and mentorship that this project has come to fruition. I am incredibly thankful to have had the opportunity to be part of his exceptional team of engineers at MTU Wave, and would especially like to thank my colleagues, Tania Demonte Gonzalez, and Houssein Yassin for their support and friendship during this season. Their collective wisdom has provided substantial insight for the development of this project in many ways, beginning with the experimental setup, and sustaining to the final technical considerations. It is without a doubt that their contributions have made this work possible.

I would also like to thank Dr. William Endres for serving on my committee, and for supporting me during my time at Michigan Tech. His counsel is of high regard, and it has been my honor to develop as an engineer under his mentorship over the years. I would like to also express my sincere appreciation also to Dr. Jungyun Bae for serving on my committee and for always believing in my capabilities. Her unfaltering compassion and support has made even the most difficult of challenges seem manageable.

Finally, I would like to thank my close family and friends, especially my father Steve Kline, my brother Ryan Kline, and our honorary sibling Damien Boron. Thanks are also in order to my dear friends Kearstin Backes and Natalie Maas. It is because of them that I have had the necessary support to persevere and conquer the things that I may never have believed to be possible.

I send my sincerest thanks to everyone who has chosen to be involved during this journey, and I will never forget the village that helped me arrive at where I am today.

Abstract

Due to the unpredictable nature of large bodies of water, wave energy can be a difficult renewable resource to rely on. One way to make Wave Energy Converters (WECs) more efficient is to apply a control strategy. In many control solutions, it is assumed that the wave excitation force is known into the future. In many instances, especially with complex waveforms, this is simply not the case. Simulation studies have shown the promise of wave force prediction using neural networks. This study demonstrates this experimentally and aims to characterize the important factors when designing such a network. Several wave elevation measurement factors are considered, including: quantity, their location relative to the buoy, and their configuration. The relationship between forecast horizon and the number of measurement backvalues is also evaluated along with both the wave form complexity and the performance impact of including instantaneous buoy acceleration. A 14.2 cm buoy, constrained to vertical motion, was subjected to 30, 60 second tests using regular and irregular waves in a wave tank. For each test its vertical motion was recorded along with an array of twelve upstream and downstream wave elevation measurements. Neural networks were trained using subsets of the data to examine the effect of the factors mentioned above on prediction performance. The results showed that upstream measurements were the most important, where the distance between the measurement and the buoy is critical. A diamond-shaped configuration of elevation measurements performed nearly the same

as using all twelve measurements illustrating the importance measurement topology. It was also found that the number of past measurements used had a significant impact on performance. Specifically, performance was best when the ratio of the prediction horizon time to the number of backvalues was one. 1 gauge far upstream, 2 gauges immediately upstream, and 1 gauge to the rear performed just as well as a full set of 12 gauges. Including acceleration as an input appeared to lower the error of most of these cases as well. It was discovered that a ratio of the forecast horizon to the number of backvalues allows the network to perform its best as this ratio is near or less than 1. Further testing is required to obtain a more complete view of the impact of waveform complexity on the results of the network.

Chapter 1

Introduction

Wave energy is a widely abundant form of renewable energy, as the planet's surface comprises mainly oceans and seas. With the help of modern technology, the energy from these perpetual waves can be harnessed and converted to electrical energy using devices known as Wave Energy Converters (WECs). Though these devices have been explored for centuries, significant improvements must be made before wave energy can become a steadfast approach in the renewable energy industry. One of the challenges that they must operate and prove reliable in unpredictable and sometimes violent sea conditions. Therefore, WECs must operate under some form of control strategy for both efficiency and self-preservation. This is to ensure reliability and to maximize energy extraction during even less-than-ideal conditions.

Such a strategy could be used whenever the surrounding wave conditions are reasonable and safe for device operation. This means that so long as the waves are viable for energy extraction and a power shutdown mode is not engaged, this resonance-encouraging control strategy will be active. This will prove to be of greater value in an incredibly rough wave field, as it can often be more difficult for WECs to reach resonance in such intense waves. During exceedingly rough conditions, many of these devices even go into a safety shutdown mode where energy collection is no longer prioritized, and preservation of the device is the objective.

1.1 Motivation

A frequent obstacle when using WEC control strategies is that some computationally expensive quantities must be known. For example, a technique such as Model Predictive Control (MPC) requires predicted, future excitation forces experienced by the WEC float (also called the buoy). This excitation force can be considered the resulting vertical force from the heaving water column below the WEC due to the waves.

With an accurate forecast of the excitation force, the control response can be computed in real time to either apply or draw energy from the WEC's generator/actuator,

called the power take-off (PTO). This timed withdrawal and deposit of energy between storage and the generator will allow the system to reach resonance as often as possible to maximize energy extraction over time.

1.2 Point Absorber Introduction

Though there are a variety of WEC architectures, this study considers only the heaving point-absorber type illustrated in Figure 1.1. These devices are designed to harness energy from the changing water pressure beneath the WEC's buoy, though some inevitable side-loading is generally tolerated. When a relative velocity $\dot{z}$ occurs between the buoy and its bottom support, power can be generated from its PTO. The extracted energy is the integral of power given by Eq. 1.1

$$E = -\int_0^t \dot{z}\, F_{pto}\, dt \tag{1.1}$$

where F_{pto} is the PTO force. When $\dot{z}$ and F_{pto} are of the same sign, the PTO is doing work on the buoy and consumes energy. When their signs are opposite, work is being done on the PTO by the buoy and energy is produced. Thus, E represents positive extraction of energy.

The resulting energy over time can either be sent directly to a load, stored as energy

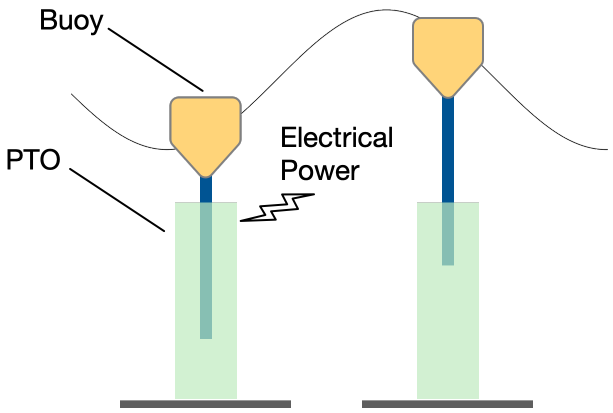

Figure 1.1: Point absorber WEC showing the buoy and power take off (PTO).

within a battery, or it can be returned to the PTO system to accommodate a control strategy. This power relationship remains the same in both circumstances of extracting energy, and for moments where a force is being applied to the system and energy is withdrawn.

1.3 Literature Review

Many researchers often proceed under the assumption that excitation force is already known, as it is often beyond the scope of the study [2]. One example of this assumption is demonstrated in a WEC study by Genest and Ringwood [3] where a pseudo spectral optimal control strategy is explored and compared to an MPC strategy.

Unfortunately, accurate, model-based estimation of excitation forces is elusive and can

be computationally expensive [4]. It has also been shown that even in linear response cases a considerable amount of error is accumulated using a model-based approach when wave amplitudes become excessive, since current models assume amplitudes of buoy motion are small. This is problematic when WECs are most productive in large amplitudes of motion.

Another limitation of current methods is the fact that most of these models solely use information collected at the site of the WEC rather than upstream wave data [2]. For a reliable real-time control implementation, the estimation of excitation force should include information of the incoming wave field instead of relying on wave measurements at the buoy. Without considering the incoming wave field, the control strategy will have very little data on what change to expect and how to reasonably cope for maximized energy extraction.

This widespread expectation of such a complicated process has led to an area of research surrounding the modeling, measurement, and prediction of wave excitation forces. Along with differential equation models, other methods to evaluate excitation forces have been explored as well.

Without the capability of measuring the force directly in an experimental setting, some studies have modeled excitation force with an augmented Kalman filter and a damped harmonic oscillator with variable frequency and damping coefficients to produce reasonable estimates [5]. However, these studies admit that there was still

error introduced due to model uncertainty. Model error was most evident among nonlinear cases, which only allowed the system to perform at about 90% of the desired efficiency.

In recent studies, more attention has been given to machine learning techniques in the search for a better solution. This has been done with simulated excitation forces using the surrounding wave field elevation measurements as inputs [6]. The study conducted by Mahmoodi et. al. found that a Nonlinear Autoregressive (NAR) network successfully forecasted such forces with simulated data, and even outperformed competitor networks, such as Long Short-Term Memory (LSTM) and Group Method of Data Handling (GMDH) networks in terms of both speed and accuracy.

1.4 Contribution

The approach described here is similar to that of [6] where a recurrent neural network was used to estimate simulated buoy motion. There are two signficant differences. First, this study focuses on wave force prediction. It will be shown in Section 2.2 that this is equivalent to predicting buoy acceleration which is similar to the buoy displacement focus of [6]. Second, this work shows the viability of the approach experimentally instead of through simulation alone as was done in [6]. This has many side results such as showing the importance of the location and geometry of wave

elevation measurements. For example, it was found that a triangular group of three wave elevation measurements performed similarly to an array of 12. In addition it was found that wave gauges behind the buoy, subjected to strong reflections and radiation, were not necessary. Instead, only measurements in front of the buoy, from the perspective of the incident wave heading, were required. These results would be extremely difficult to uncover with simulations, short of using computational fluid dyanmics (CFD) solvers.

Chapter 2

Point Absorber Modeling and Force Prediction

To form a control strategy, a mathematical model of the WEC is often helpful. The model described below considers all forces affecting the WEC's motion from the surrounding wavefield and if present, a control force from the PTO. WECs behave differently depending on the amplitude and complexity of the imposing wavefield and often need to be described with one of two different models. When a WEC experiences small amplitude oscillations it follows a linear model, while greater motions require a nonlinear modeling approach. After summarizing a typical point absorber model, the problem of predicting wave forces is converted into predicting acceleration when the buoy's added mass is known.

2.1 Point Absorber Model

The general differential equation model of a point absorber is the sum of the forces on the buoy from the wavefield and a PTO force, F_{pto} shown in Eq. 2.1

$$m\ddot{\zeta} = F_{fk,st}(\zeta,\eta) + F_{fk.dy}(\zeta,\eta) + F_d(\eta) + F_r(\dot{\zeta}) + F_{pto} \tag{2.1}$$

where m is the buoy mass, ζ is the vertical buoy displacement and η is the wave elevation relative to the still water line. A few of these forces are quite simple to calculate and measure such as the buoy weight, F_g, and F_{pto}. The PTO force is generally known as this is the force commanded by the control strategy. The product of F_{pto} and $\ddot{\zeta}$ is the work rate done to or by the WEC. If this product is negative, then work is being done on the WEC by the waves. In contrast, if the sign is positive, then the WEC is doing work on the water. The objective of a WEC control strategy is to maximize the work done by the water. This may come at the expense of small amounts of energy, but the returns from this action can be far greater than this loss.

The hydrostatic Froude-Krylov force, $F_{fk,st}(\zeta,\eta)$, is the difference between the force from gravity and the Archimedes force from static pressure on the WEC float, $\rho g V$ where ρ is the water density, V the displaced volume and g the gravity acceleration [4]. Because the buoy's shape, and mass properties are known, the expression is

simple to calculate for small waves, yet may be nonlinear due to the buoy's geometry. In general, it's a nonlinear function of η and ζ.

The dynamic Froude-Krylov force, $F_{fk,dy}(\zeta, \eta)$ captures the force due to the varying pressure distribution on the buoy's wetted surface due to waves passing by it. Giorgi and Ringwood developed a strategy for creating a closed form expression for axisymmetric buoys, including a sphere. They further concluded that for a sphere experiencing small motion, its effect is negligible [4].

The diffraction force, $F_d(\eta)$, represents interfering forces on the buoy when the wave field is forced to encounter an obstacle, in this case, the buoy itself. Such an obstacle will encourage wave propagation and could increase disturbances to the system. If the incident wavelength is large with respect to the buoy diameter, then the diffraction force is considered negligible.

The radiation force $F_r(\dot{\zeta})$ of Eq. 2.2 is due to transfer between the buoy's kinetic energy and the water. This is the same force that causes a ripple effect radiating outward from a pebble when dropped into a still pond. The linear form of the radiation force has two terms: one being a function of velocity $\dot{\zeta}$ and the other a function of acceleration $\ddot{\zeta}$.

$$F_r(\zeta) = -\bar{a}_\infty \ddot{\zeta} - \int_0^\infty h_r(\tau)\, \dot{\zeta}(t-\tau)\ d\tau \tag{2.2}$$

where $\bar{a}_\infty$ is the constant added mass and $h_r(\tau)$ is the radiation impulse response function. Both terms depend on the buoy's shape and its draft line and are well known. An article from Havelock showed analytically that for a sphere, $\bar{a}_\infty$ is equal to one-half of the physical mass of the object when the draft line is located at the geometric center [7]. This added mass varies when the draft line of the sphere is no longer located at the geometric center, but plenty of techniques exist to find this value.

By substituting Eq. 2.2 into Eq. 2.1, the WEC differential equation model can be written as:

$$\begin{aligned}(m+\bar{a}_\infty)\ddot{\zeta} = \; & F_{fk,st}(\zeta) + F_{fk,dyn}(\eta,\zeta) + F_d(\zeta) - \int_0^\infty h_r(\tau)\,\dot{\zeta}(t-\tau)\,d\tau + F_{pto} \\ = \; & F_w(\eta,\zeta,\dot{\zeta})\end{aligned} \tag{2.3}$$

where F_w will be termed the total force. The reason for including the expression for the radiation force, is to show the impact of the effective mass, $m+\bar{a}_\infty$. It's important to note that Eq. 2.3 is subject to many assumptions, including small motion. Though approximate, the form of the model, indicated by a general dependence of F_w on η, ζ and $\dot{\zeta}$, is assumed to be correct.

2.2 Force Prediction

This work uses accumulated data of buoy motion and wave elevation to predict the total wave force, F_w at some future time, t_1, or $F_w(t + t_1)$. In this case, it is unnecessary to distinguish each individual force on the buoy which means the model can be described in much simpler terms. Under the assumption that the added mass is known, the problem can be transformed into a direct estimation of the buoy acceleration, $\ddot{\zeta}$ rather than the total wave force F_w. Solving Eq. 2.3 for acceleration, we get Eq. 2.4.

$$\ddot{\zeta} = \frac{F_w}{(m + \bar{a}_\infty)} \tag{2.4}$$

One approach to estimating $F_w(t + t_1)$ would be to use present and back values of $\ddot{\zeta}$ to extrapolate forward in time, and then compute F_w using m and $\bar{a}_\infty$. However, the the excitation of the buoy due to unknown, future waves is completely ignored and would lead to signficant errors for any but small t_1 values. The neural network introduced in Chatper 3 will be trained to predict $\ddot{\zeta}(t + t_1)$ for t_1 seconds in advance over a broad range of η and ζ conditions, explicitly considering the excitation from waves.

To achieve predictive capability, strategically placed upstream wave elevation measurements could provide the network additional information about the forces that

are soon to accelerate the buoy. An instantaneous snapshot of these measurements, including the buoy's instantaneous acceleration will be given to the network as training data. For most cases, this input will need to include a series of multiple back values for each measurement to properly provide enough infotmation for the network to observe the changing trends in the buoy's response. The configuration of inputs will be described when the input and target are discussed.

Wave speed will also be considered for the experimental setup. The wave speed helps determine the time it takes for a wave to travel from the wave gauges to the buoy. This is helpful because it can provide insight on what the wave elevation may be just moments ahead at the site of the buoy.

For a single frequency, regular wave its wavelength λ, period T and water depth, h are related through the dispersion equation

$$\lambda = \frac{gT^2}{2\pi} \tanh\left(2\pi \frac{h}{\lambda}\right) \tag{2.5}$$

and its wave speed is $c = \frac{\lambda}{T}$. If the water is deep compared to the wavelength, or $\frac{h}{\lambda} >> 1$, then the wavelength can be approximated as shown in Eq. 2.6.

$$\lambda \approx \frac{gT^2}{2\pi} \tag{2.6}$$

and the wave speed can be approximated as

$$c \approx \frac{gT}{2\pi} \tag{2.7}$$

It will be shown later that wave speed is an important factor to determine the number of back values needed to estimate future buoy acceleration.

Since a buoy's motion also produces its own waves, it's likely that several wave elevation measurements are needed in the vicinity of the buoy. When considering gauge location placements, upstream data is thought to provide more information about the changing wave forces to come and downstream measurements are thought to provide more insight to the buoy's own waves that result from its oscillation. It is assumed that some combination of these locations will prove to be better than others.

In the subsequent sections, a solution is proposed to use a neural network to learn the behavior of a passive heaving sphere, $F_{pto} = 0$, given a variety of incoming wave conditions. The intention is to train a network to make predictions about future buoy acceleration so that model predictive control (MPC) strategies may be used that rely on knowledge of future wave forces. Under active control, $F_{pto} \neq 0$ however, since when implementing MPC, F_{pto} is known for some time into the future the component of $\ddot{\zeta}$ associated with F_w can be combined with the acceleration prediction during the

control solution process. For example, let's define F_{net} as

$$F_{net} = (m + \bar{a}_\infty)\ddot{\zeta} = F_w + F_{pto} \tag{2.8}$$

where we assume that F_{pto} is known into the future as part of the MPC solution process and we also know the predicted $\ddot{\zeta}$. Then the wave force can be predicted as

$$F_w = (m + \bar{a}_\infty)\ddot{\zeta} - F_{pto} \tag{2.9}$$

Chapter 3

Neural Network Acceleration Prediction

After a brief introduction to neural networks, including the inputs and outputs used for acceleration prediction, the experimental setup is described that was used to acquire training and testing data.

3.1 Neural Network Introduction

Consider the neural network illustration of Figure 3.1 showing the input, hidden and output layers. The input layer, as the name implies, contains the input data, also

called the predictors. Determining the number and quantities to use as predictors is a significant aspect of neural network design and should correlate to the outputs, contained in the output layer. The in-between hidden layer(s) are where the processing happens, as information flows from one layer to the next.

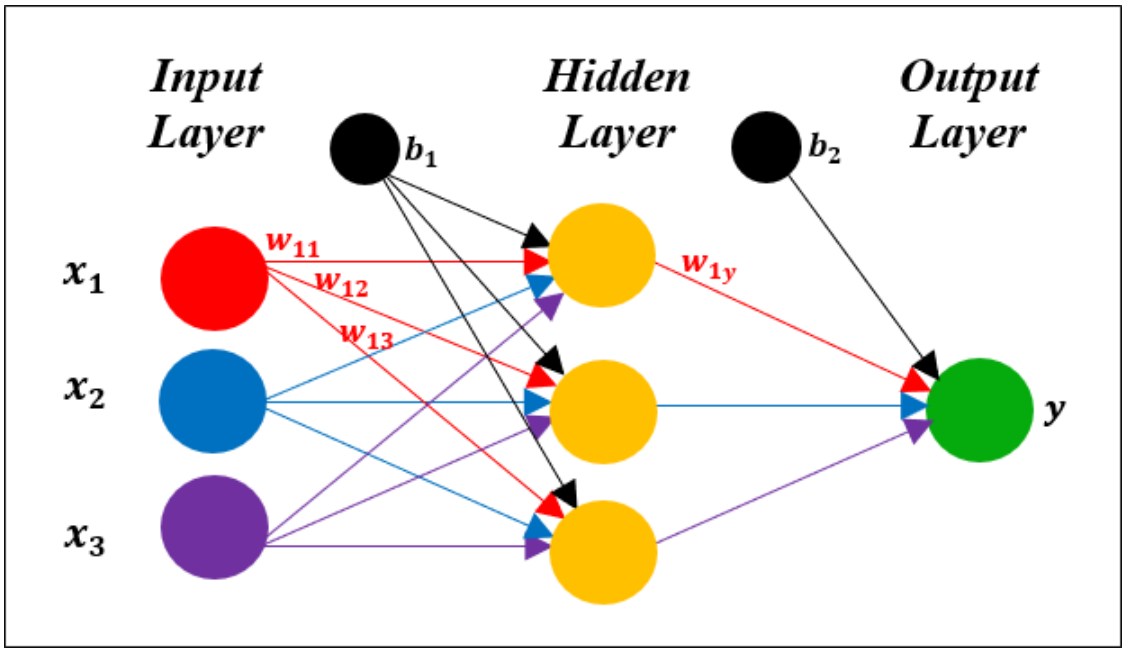

Figure 3.1: The basic architecture of a neural network, where weights and biases are applied to each neuron.

The output of each neuron is calculated as shown in Eq. 3.1 and passed on to become the input to the next hidden layer, or the output.

$$y_k = f\left(\sum_{j=0}^{m} w_{kj}x_j + \ b_k\right) \tag{3.1}$$

The input provided from the previous neuron in layer j, is denoted x_j and $w_{k,j}$ is the weight from layer j to k. The bias is denoted b_k, and y_k is the output at the kth

neuron. The activation function, f, operates on the linear combination of x_j and b_k and is selected based on the problem. Creating an appropriate activation function is another aspect of the neural network design process and can range from linear to nonlinear. The terms 'predicting series' and 'input series' will be used interchangeably to represent the independent inputs of the problem. Using this predicting series, the network should aim to match the 'Target Series' as closely as possible, which is made of the dependent variable data that the network would be trained to predict. Neural networks sometimes use a series of back values that can be defined by the user to allow the network access only to the most relevant and recent information both in training with the target series, and in operation where only the predicting series is involved. These back values allow the network only to see the most recent information and to hopefully spot changing trends. Both the target and predicting series will be combined into one comprehensive input, and the result will be divided for both training and testing purposes. For training, the target series is used to establish the weights and biases necessary for the network to make accurate predictions. The network determines these weights and biases to achieve a minimal overall error between the target series and network response. When testing, only the predicting series is given to the network, and the weights and biases determined from training can remain intact during operation. In this situation, the target series may be used to determine the accuracy of the network output.

For buoy acceleration prediction, the inputs consist of available wave elevation and

buoy acceleration. Buoy acceleration will always be the current and previously measured values. In contrast, the wave elevation options are numerous with variations in location, and number. Many combinations of these inputs will be explored and used to compare neural network performance. One of the contributions of this work was the discovery that a small number of gauges in a traingular formation yielded similar results to a large grid of gauges. Buoy acceleration prediction, at a specified horizon t_1, is the single response variable.

The act of training a neural network is the calucation of the weights and biases such that the neural network output matches the responses of the training data set. This is accomplisehd using numerical optimization and has similarities to system identification of parameters in differential equation models.

3.2 Training Data Acquisition and Processing

After a brief introduction of the wave tank, the experimental setup is described along with the wavefields used to train the network.

3.2.1 MTU Wave

Michigan Tech's Wave Tank Laboratory, MTU Wave, hosts an 8,000-gallon freshwater wave tank designed by Edinburgh Designs. The tank is three meters wide, ten meters long, and one meter deep, with a maximum wave height, trough-to-peak distance, of 0.25 meters. For ease of access to any part of the tank, there is an overhead bridge that may be positioned as desired. On one end of the tank, there are eight position and force controlled paddles that are used for generating waves. These paddles are vertical at rest, but can rotate about their bottom hinge by ± 40 degrees, with the ability to create a wide range of wave scenarios from 0.5 to 2.0 Hz. Since the paddels are both position and force controlled, they can provide damping to help the tank achieve steady state after the paddles stop moving making it possible to collect many waveform measurements back-to-back with minimal settling time in between.

There will always be some amount of reflection and wave interaction with the tank itself. There is a limited amount of time from the beginning of wave propagation until wave reflections from the walls of the tank can significantly disturb the true waveform shape, about 20 to 40 seconds. To reduce this effect and prolong the window of disturbance-free data collection, the opposite end of the tank has an energy-absorbing "beach". These reflections will be greatly reduced, but never absent, and therefore must be considered during neural network training. The beach in this tank is a steel

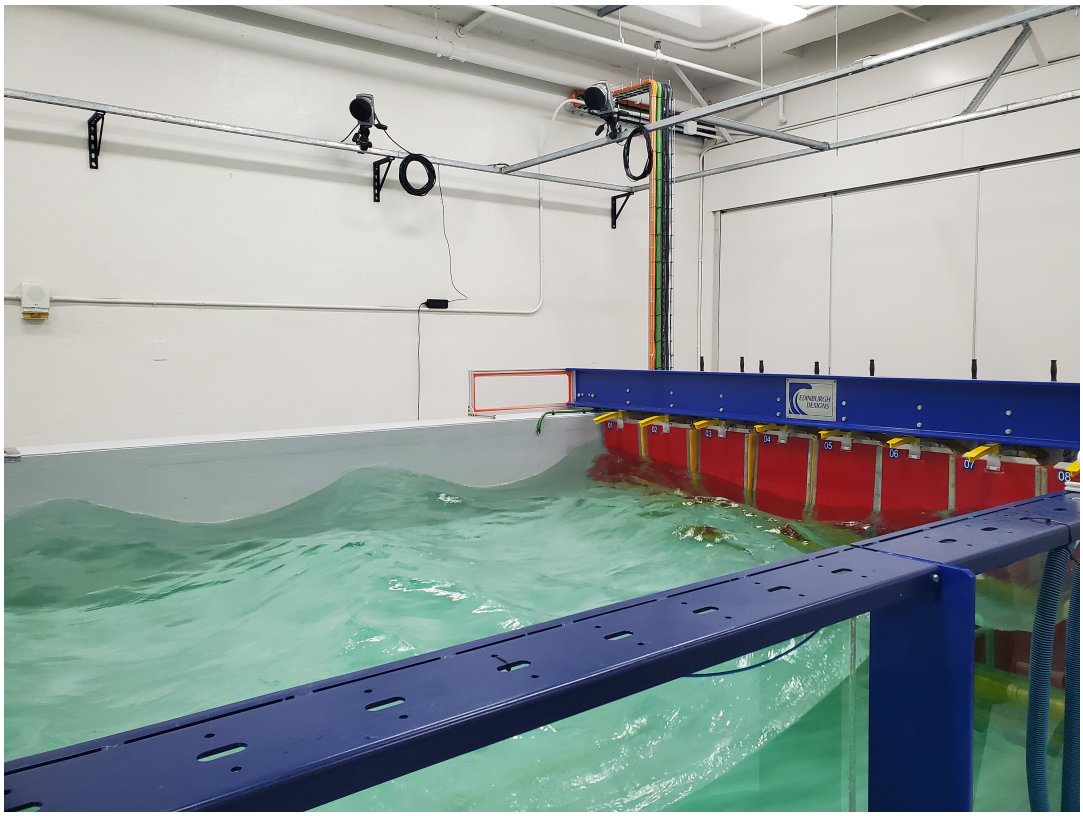

Figure 3.2: The Michigan Tech wave tank performing a simulation.

structure with a durable polyethylene paneling that is bolted to the frame. This energy-absorbing quality is due to the angle and curvature of the beach, which is specifically designed according to the operational water depth of this tank.

3.2.1.1 Wave Gauges

Twelve Edinburgh Designs resistive wave gauges, shown in Figure 3.3, were used to measure wave elevation. They consist of two probes that dip into the water. As the wave elevation changes, the probe resistance changes and is extracted from the

excitation voltage using a bridge signal conditioner. After a four-point calibration, the gauges provide an output voltage proportional to the wave elevation with ±1 mm uncertainty.

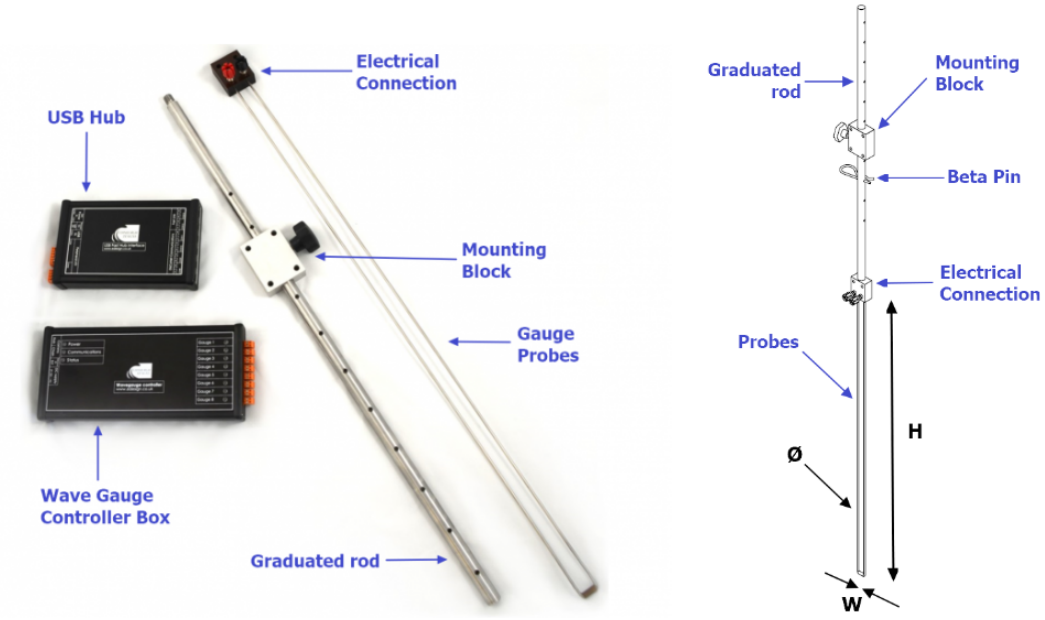

Figure 3.3: An Edinburgh Designs resistive wave gauge [1].

3.2.1.2 Qualisys Motion Tracking System

MTU Wave is equipped with eleven, 180 frame per second, infrared motion-tracking cameras as part of the Qualisys system and was used to calculate buoy acceleration. The cameras are suspended on beams above the tank, where the location of reflective markers can be tracked with ±2 mm uncertainty, depending on the quality of the system's calibration and location of the markers. Preparing the Qualisys acquisition

system, Qualisys Track Manager, for a test requires a significant amount of customization. For example, software "region masking" must be performed for each camera to reduce unwanted reflections by blocking out a designated area from the field of view. There are drawbacks to the over-use of this feature, as it can cause a large area to be undetectable, limiting the tracking workspace. In addition to masking, there are other features that can make the markers and reflections more, or less visible such as the image intensity. This can allow for much cleaner data collection, as strategic modification of these settings will help determine the threshold for what is seen as a 'marker' and what is simply a stray reflection to be ignored.

3.2.1.3 Data Acquisition and Synchronization

The Qualisys motion tracking system and the Edinburgh Designs wave gauges have separate logging systems. One hurdle that needed to be addressed was the synchronization of measurements from both Qualisys and Edinburgh Designs instrumentation. Because the Windows operating system that governs the Edinburgh Designs software does not work in real-time while Qualisys software does, it was necessary to use a common control system to execute the initiation of measurements and paddle start/stop commands. The digital I/O of a dSPACE MicroLabBox was used to communicate between systems with a custom dSPACE Control Desk application.

The dSPACE MicroLabBox was programmed to receive a signal from the Edinburgh

Designs interface box, indicating that the paddles had started and wave elevation was being measured. When this event occurred, the dSPACE box sent a digital output, one millisecond later, to the cameras' controller to trigger the recording of data in Qualisys Track Manager. This ensured that the buoy position and wave elevation data were properly aligned. For this study, data was captured at 128Hz from all the logging devices. For ease of processing, the data was downsampled to 20Hz.

3.2.1.4 Wave Design Software

The Edinburgh Designs Njord Wave Sysnthesis application was used to aid wave field design for the tests performed to produce the training data, each 60 seconds in duration. After specifying a wave field's frequency content, the paddle commands are generated and saved to a file, allowing experiment repeats to be performed reliably simply by executing the save paddle command file.

3.2.2 Experimental Setup

The experiments made to collect training data used 12 wave gauges and a spherical buoy with a through hole, illustrated in Figure 3.4. The buoy's properties are summarized in Table 3.1. To restrict the buoy from horizontal motion and to allow free vertical motion, a rod was placed through its center hole and mounted to the

overhead bridge. Because both the rod and surface of the buoy were quite smooth, and the through hole had 5mm of clearance, the friction was considered negligible. Drop tests were performed and the buoy response on the rod was nearly identical to the response without the rod.

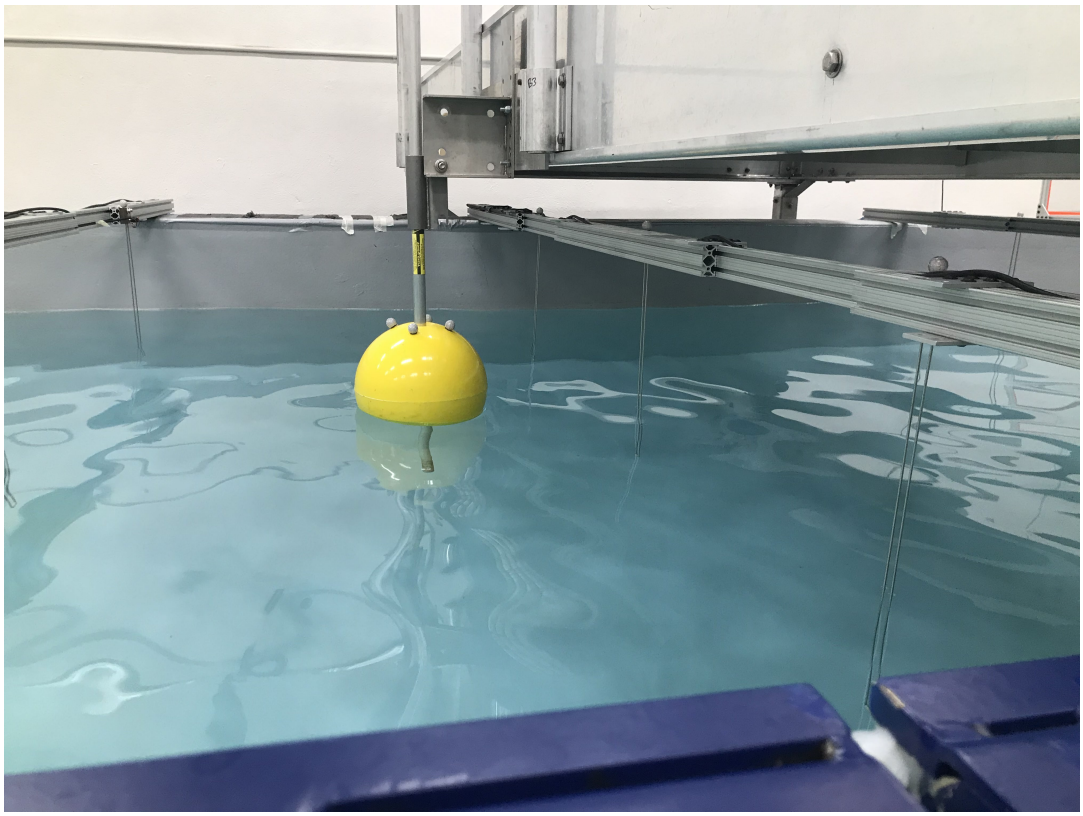

Figure 3.4: The yellow buoy has a 1 inch through-hole that can allow it to become constrained to its position in the horizontal plane with the help of a vertical rod.

Wave gauges (shown as blue dots in Figure 3.5) were placed around the buoy (gray circle), and were numbered both indivdually and by group. Each wave gauge group was attached to the same mounting beam, and therefore the incoming waves hit each gauge in the group at approximately the same time. The layout was designed

Table 3.1
Buoy properties.

Property	Value
Radius, cm	14.20
Mass, kg	2.72
Added Mass, kg	1.14
Draft, cm	9.00

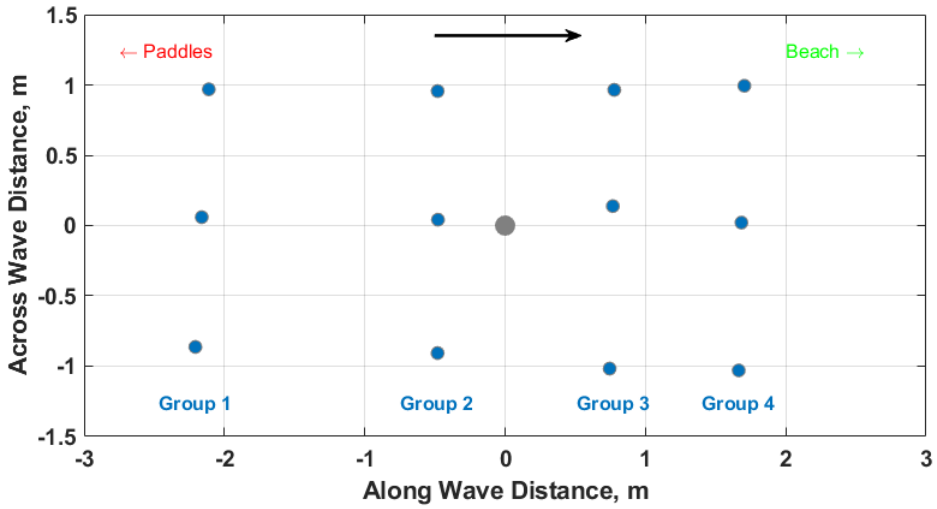

Figure 3.5: The buoy is at (0,0) with the wave direction from left-to-right. Wave gauge locations and vertical groups are shown as smaller circles.

to permit exploration of both near and far wave elevation measurements. It was anticipated that the groups nearest to the buoy (groups 2 and 3) would be helpful in determining the buoy response, while the gauges further upstream would extend the prediction horizon. The gauges in group 4 were downstream of the buoy to measure

wave reflections. This was important since the tests were performed in a finite-domain tank, with wave reflections present. The precise locations of these gauges can be found in Appendix B.

Four markers were placed at the top of the buoy and tracked by the Qualisys system. The initial location of the buoy in the tank was calibrated under still-water conditions. Similarly, markers were placed atop the wave gauge mounting locations to calibrate their locations relative to the buoy to within about 2 mm.

Because infrared cameras rely on tracking the reflective markers, any other reflective surface within view poses a threat to the accuracy and detection of marker tracking. To combat this issue, physical masks were posted over unwanted reflections. Software masks were also applied using the Qualisys Tracking Management application.

3.2.3 Training Data Tests

A variety of waves were explored for network testing and training. These waveforms vary in number of frequencies, amplitudes and speeds. It was thought that by providing a mixture of both simple and complex waveforms, the neural network would be able to accurately predict buoy behavior over a broad spectrum of situations.

Ten waveforms were designed, summarized in Table 3.2, using the Njord Wave Synthesis application with frequencies ranging from 0.4 to 1.0 Hz and significant wave heights from 0.13 m to 0.24 m. Nine waves were irregular, with n frequency components, and one was regular. Since irregular waves cannot be characterized by a single amplitude, period or speed, the 1/3 significant values of height, $H_{1/3}$, period, $T_{1/3}$, wavelength, $\lambda_{1/3}$ and speed, $c_{1/3}$ are provided. The Speed column shows a relative description of wave propogation speed as S (slow), M (medium) and F (fast). There is more information about these waveforms in Appendix A.

Table 3.2
Wave field characteristics for the training data tests.

#	n	Frequencies, Hz,	$H_{1/3}$, m	$T_{1/3}$, s	$\lambda_{1/3}$, m	$c_{1/3}$, m/s	Speed
1	5	0.50 0.70, 0.80, 0.90, 1.00	0.30	1.29	2.58	2.01	S
2	5	0.20, 0.55, 0.75, 0.80, 0.85	0.15	1.30	2.64	2.03	S
3	3	0.50, 0.70, 1.00	0.24	1.42	3.16	2.22	S
4	4	0.20, 0.55, 0.80, 1.00	0.15	1.61	4.06	2.52	M
5	4	0.40, 0.60, 0.75, 1.00	0.20	1.64	4.21	2.56	M
6	2	0.50, 0.60	0.24	1.78	4.95	2.78	M
7	3	0.40, 0.50, 0.86	0.17	2.17	7.35	3.39	F
8	1	0.45	0.18	2.22	7.71	3.47	F
9	3	0.40 0.50, 0.90	0.19	2.23	7.79	3.49	F
10	2	0.40, 1.00	0.13	2.26	8.00	3.54	F

Thirty tests were performed where the ten waves of Table 3.2 were each repeated three times. Due to being incredibly identical, only 1 of each type were used, resulting in the selection of these 10 waveforms. Buoy position and 12 wave gauges were recorded during each 60 second experiment using the synchronization method described in section 3.2.1.3. Acceleration was calculated from buoy position data using a 4th

order, low-pass, Butterworth filter, with a 1.59 Hz (10 rad/s) cutoff frequency along with a $\Delta z/\Delta t$ derivative.

A sample set of data is shown in Figure 3.6, demonstrating both a filtered, and unfiltered buoy response for waveform 1.

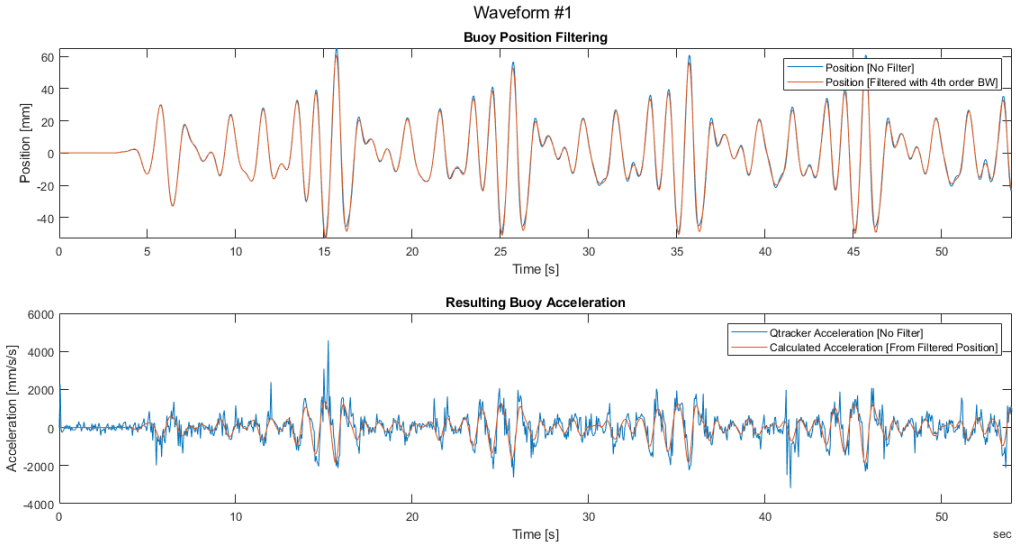

Figure 3.6: Sample data set from test wave number 1, showing filtered and unfiltered buoy acceleration and position.

Chapter 4

Neural Network Training and Results

As described earlier, there are several aspects in designing the neural network acceleration predictor, including the inputs (location and number of wave gauges), the number of hidden layers, and the number of accessible backvalues. It should be noted that using too many hidden layers may result in overfitting since each hidden layer introduces more free variables that must be found during the training process. For the tests belonging to this study, only 2 hidden layers will be used. In addition, the tests from sections 4.1 - 4.5 will be performed for a forecast horizon t_H of 1 second and 5 backvalues.

One of the objectives of this work was to understand if a fine grid of wave elevations is required for accurate acceleration prediction. Naturally, there will be some combination of gauge inputs, and network settings (forecast horizon and the number of backvalues) that will produce a more successfully trained network than others. To determine which aspects are most helpful, various cases were evaluated with different combinations of these inputs and network settings to design an acceleration predictor. The resulting network performance from applying these predictors will be compared across cases to determine the impact of each aspect. For all the following test cases, the metric used to quantify network performance was the average root mean square of measured and predicted acceleration at the horizon time t_H. These performance metrics will be used in comparison to one another to gather conclusions about what should be considered when designing a neural network acceleration predictor. We will call each aspect a 'factor of interest', and these factors will be explored in the test cases described in this section.

The factors of interest considered were:

1. The effect of upstream and downstream wave gauges
2. The distance of wave gauges to the buoy relative to the wave speed
3. Wave gauge topology, e.g. triangular versus a line
4. The quantity of wave gauges
5. The effect of using the buoy's instantaneous acceleration, $\ddot{\zeta}$, in the input set

6. The relationship between forecast horizon, N_H, and the number of back values N_B.

7. The network accuracy relative to the complexity of the waveform

For each of these factors, several test sets were created to explore its effect. A neural network was trained for each case using seven of the ten training data sets. The remaining three cases were used to evaluate performance. The intention is to determine the influence of the factor, so that there is a better understanding of how to design a measurement set for acceleration prediction.

Due to the optimizing nature of a neural network, the results from running a test case more than once will be similar, but not identical. This is because the optimization scheme is searching for the ideal values for weights and biases to reproduce the target, and therefore could find multiple valid solutions. These tests were performed multiple times to ensure that a representative sample was used to discuss and evaluate the factor of interest.

4.1 Up and Downstream Wave Gauge Locations

Three cases, described in Table 4.1 and illustrated in Figure 4.1, were created to understand the impact of upstream and downstream wave elevation measurements

on acceleration prediction. After a description of the reasoning behind the cases, the results of trained neural networks are provided.

4.1.1 Case Descriptions

Upstream wave gauges are the first to experience any changes in wave elevation that would translate into a change in buoy acceleration. In contrast, downstream measurements receive information after the wave has already passed by the buoy. Because of this interaction, there may be minor disurbances in the wave field that could provide information about how the buoy's self-made waves have altered the wave field between the upstream and downstream gauge measurements. In addition, downstream measurements were also anticipated to have important information from reflected waves. By including both upstream and downstream measurements, a full view of the wavefield is available to the acceleration predictor.

Consider the three cases described in Table 4.1 and visualized in Figure 4.1. Cases A and B consist of six gauges each, where A includes the upstream gauge groups 1 and 2, and B uses the downstream gauges in groups 3 and 4 of Figure 3.5. Case C uses all 12 wave gauges and is assumed to provide the best performance.

Table 4.2 shows the subset of three waves, from Table 3.2, used to explore upstream versus downstream measurement location. The waves were selected based on their

Table 4.1
Cases used to evaluate the effect of downstream and upstream wave gauge location on acceleration prediction.

Case	Gauge #s,	Location	Purpose
A	1-6	Upstream	Upstream/Downstream Effect
B	7-12	Downstream	Upstream/Downstream Effect
C	1-12	All	To test the full set

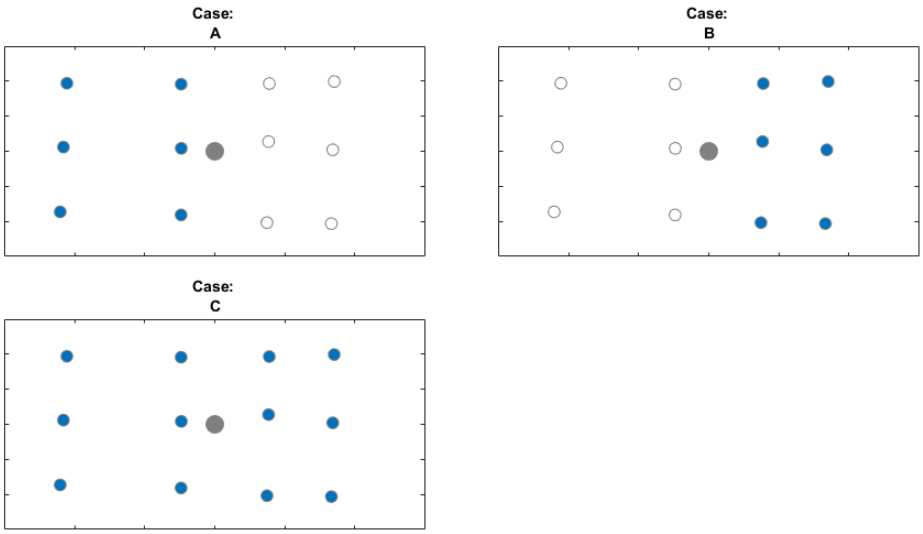

Figure 4.1: Illustration of the wave gauges used for the cases described in Table 4.1 where waves propogate from left-to-right.

speeds - slow, medium and fast, and will be used again in Sections 4.2 through 4.5.

To evaluate the three gauge location cases of Table 4.1 for each of the three waves of Table 4.2, nine neural networks were trained, whose performance is described below.

Table 4.2
Waves from Table 3.2 that are used to explore the factors of Sections 4.1 through Section 4.5 based on wave speed.

Waveform #	$c_{1/3}$, m/s	Classification
1	2.01	S
5	2.78	M
10	3.54	F

4.1.2 Results

The results of the nine networks are shown in Figure 4.2. Interestingly, Case A, performed similarly to, and even slightly exceeded the performance of case C despite only having six gauges upstream from the buoy. This indicates that perhaps downstream gauges are not as important to include for an acceleration predictor, and could perhaps even introduce additional error to the network results. Case B, including six downstream gauges, resulted in significant error, and could not track the target acceleration data. This confirms the hypothesis that upstream gauges are more valuable in a forecasting setting than downstream gauges, regardless of wave speed. This is not to insinuate that downstream gauges are irrelevant; their effect will be further explored in the subsequent sections.

Figure 4.2 is the first of many subsequent plots of using the root mean square error metric to evaluate prediction performance. To help provide insight into the relationship between the RMSE value and prediction performance, consider the results

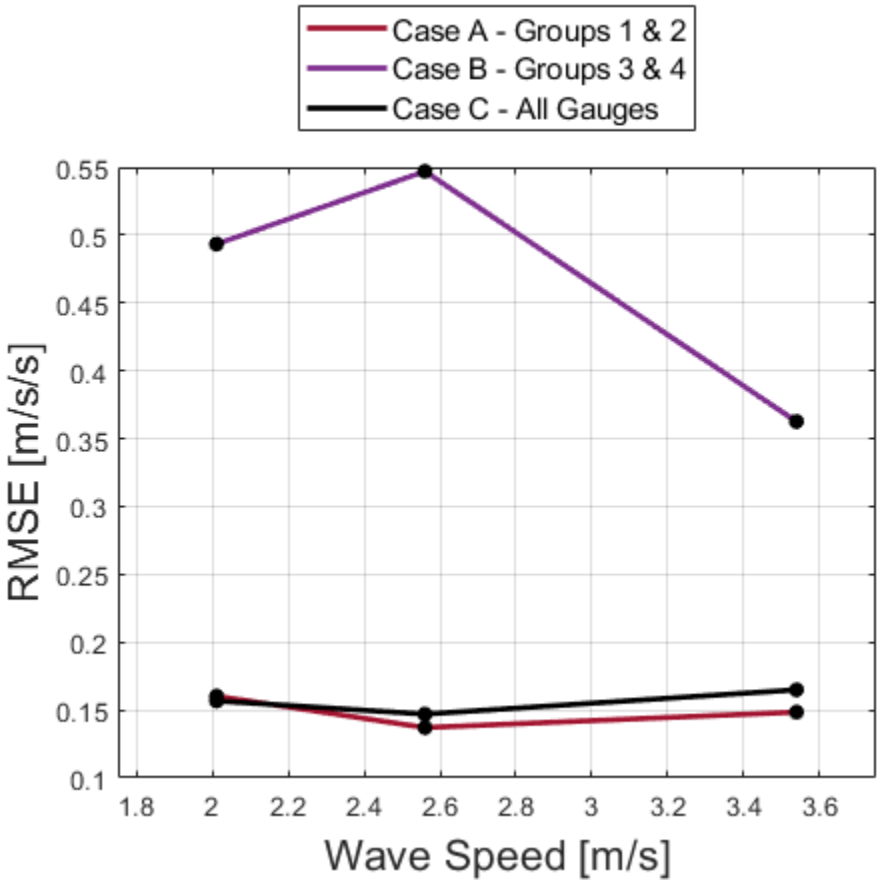

Figure 4.2: Acceleration prediction performance comparison of upstream gauges (Case A), downstream gauges (Case B) and all gauges (Case C).

of Figures 4.3 through 4.5. Each figure contains an overlay of the measured and network-predicted buoy acceleration one second into the future using wave field one. From Figure 4.2 the RMSE metrics are about 0.14, 0.55 and 0.15 for these cases (A through C, respectively). The RMSE is greatly affected when there is a mismatch in frequency content and phase as illustrated by Figure 4.4. In a rather subjective way we can see that RMSE < 0.2 yields a reasonable match while RMSE > 0.5 results in a poor prediction.

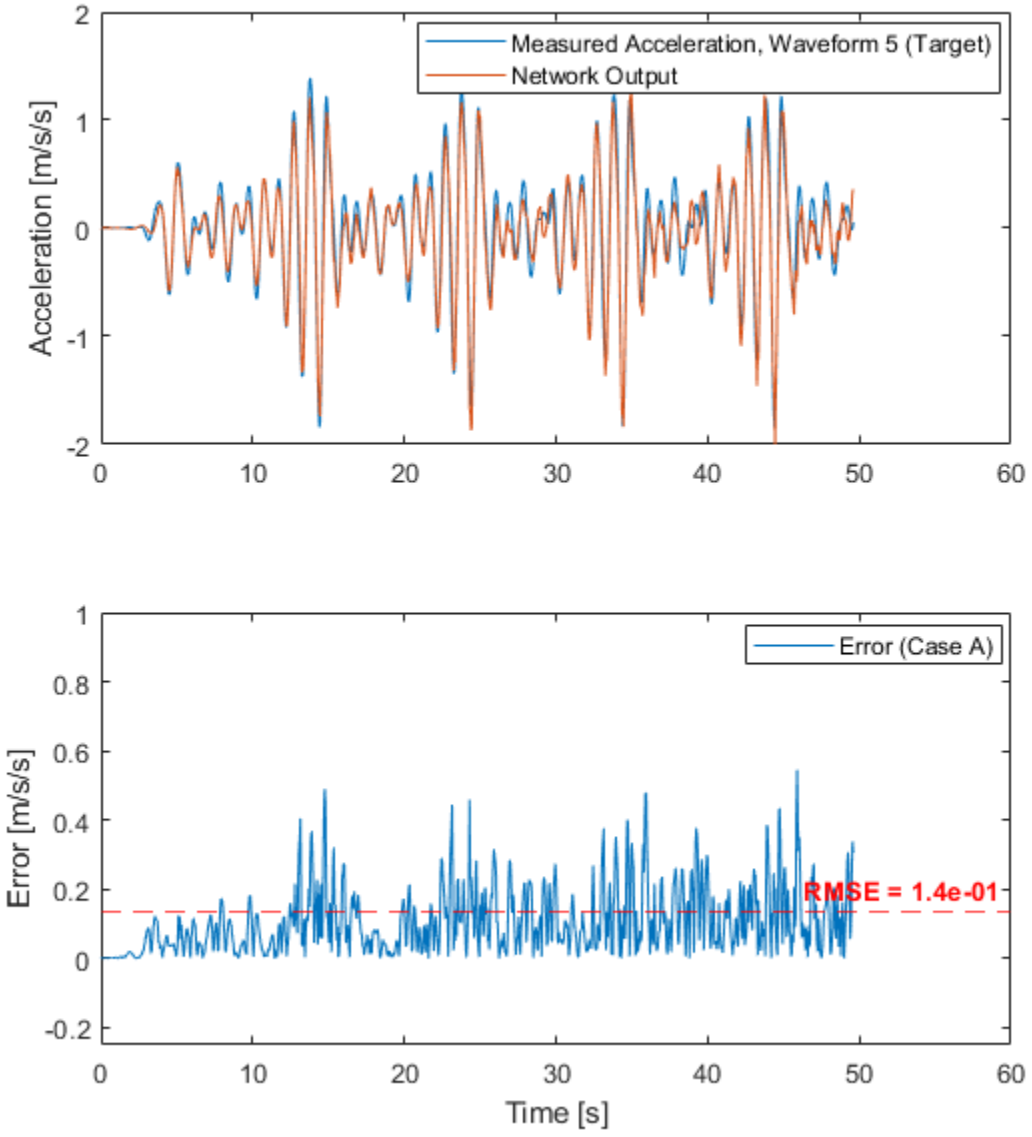

Figure 4.3: Comparison of measured and network-predicted acceleration for waveform 5 and test Case A, and the associated error.

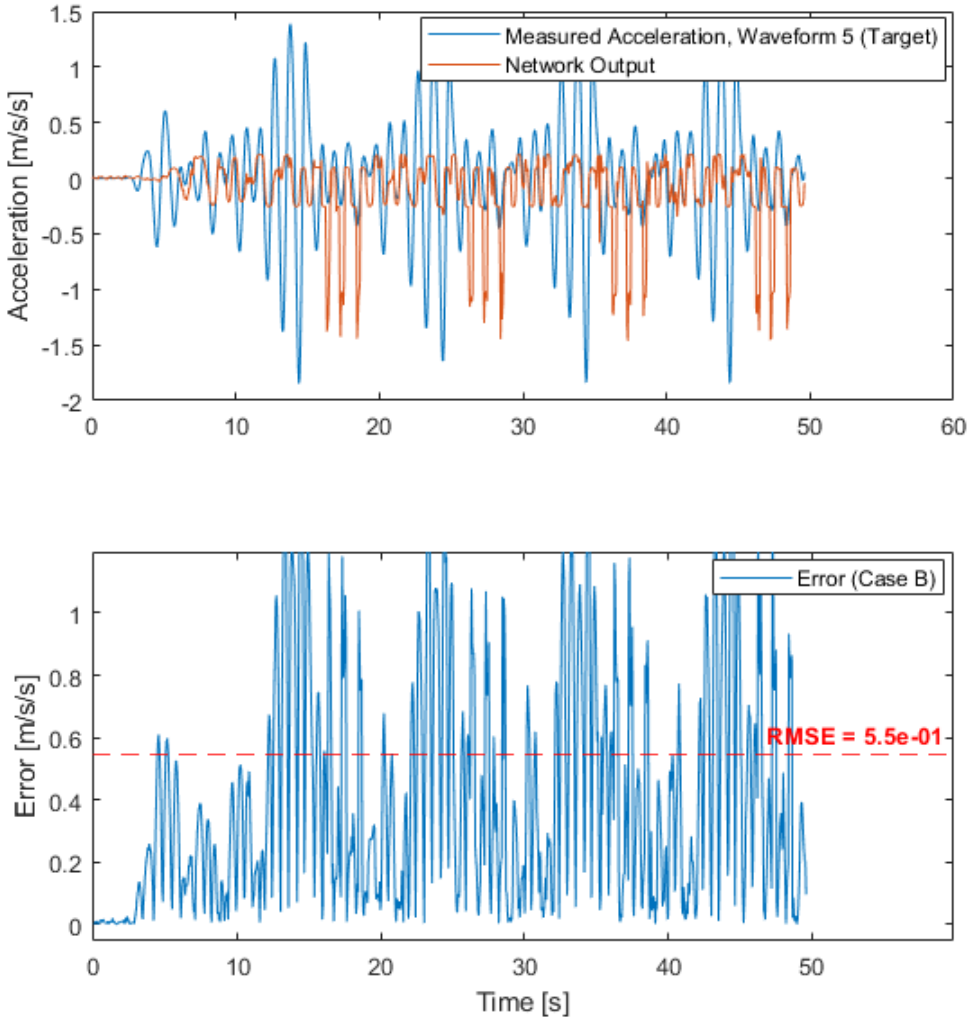

Figure 4.4: Comparison of measured and network-predicted acceleration for waveform 5 and test Case B, and the associated error.

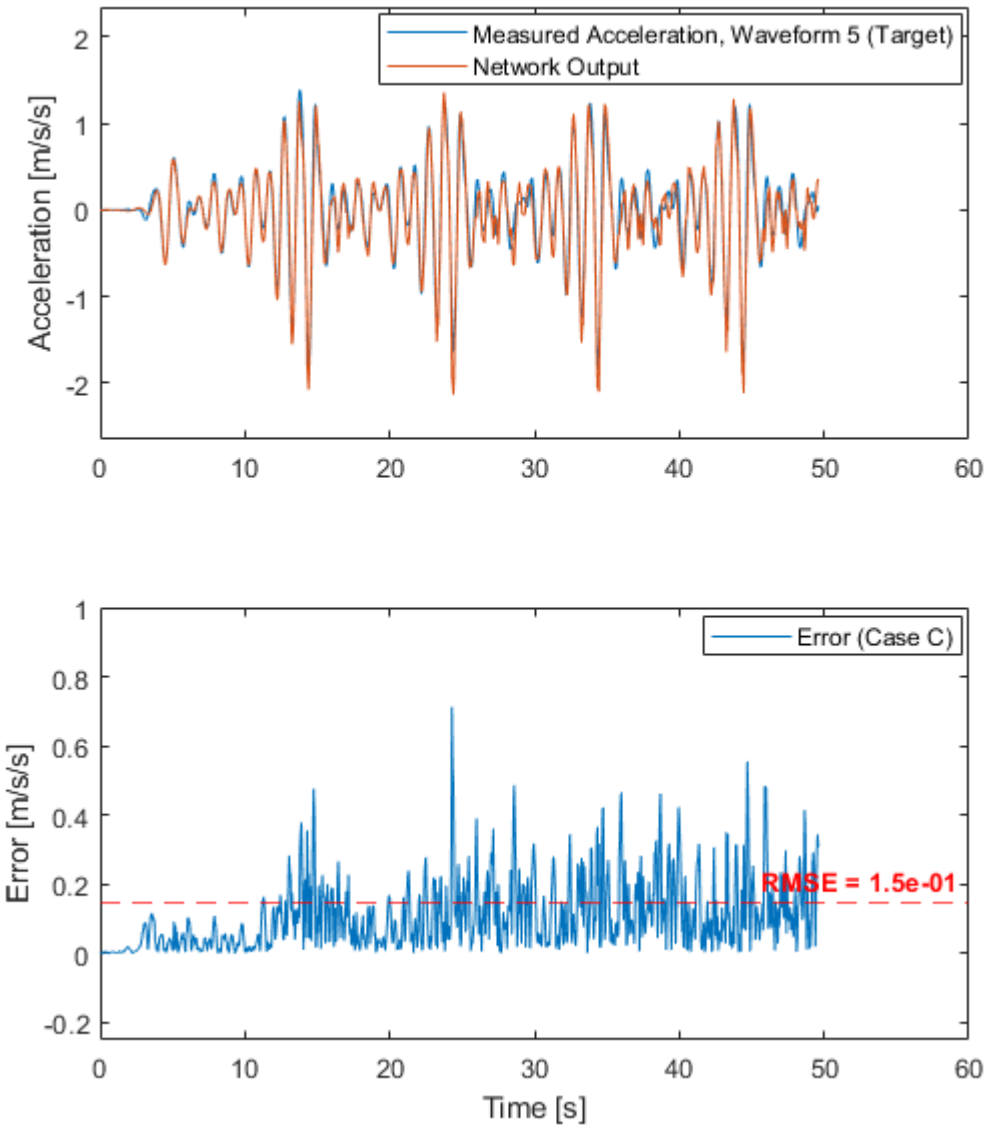

Figure 4.5: Comparison of measured and network-predicted acceleration for waveform 5 and test Case C, and the associated error.

4.2 Wave Gauge Location and Wave Speed

Eight cases, described in Table 4.3 and illustrated in Figure 4.6, were created to understand the impact of wave gauge location and wave speed on acceleration prediction. These cases include single wave gauges, as well as lines of wave gauges at different distances from the buoy. After a description of the reasoning behind the cases, the results of trained neural networks are provided.

The placement of the gauges relative to wave speed may also prove to impact the ideal number of back values the network should be given. If a waveform has a very low frequency (large wavelength), it may need a longer snapshot to capture the trends in the changing measurements. Conversely, a higher frequency (small wavelength) might only need a brief number of back values to capture the waveform. This effect is explored in more depth later in section 4.6.

4.2.1 Case Descriptions

Depending on the speed of the incoming wave, gauge placement may serve to be important in making accurate predictions. For example, for a wave with a much higher speed, it may be reasonable to want a measurement quite a bit further upstream to

have more time before the wave reaches the buoy. This added distance may also allow for greater forecast horizons for slower waveforms. Therefore, the effect of wave speed will be considered using the same waveform test cases used previously, shown in table 4.2.

The eight cases of Table 4.3 are divided into single and multiple wave gauge categories, Cases D-G and H-K respectively, and are illustrated in Figure 4.6.

Table 4.3
Cases used to evaluate the effect of gauge proximity to the buoy and their number

as illustrated in Figure 4.6.

Case #	Gauge #s,	Location
D	2	Far Upstream
E	5	Close Upstream
F	8	Close Downstream
G	11	Far Downstream
H	1-3	Far Upstream
I	4-6	Close Upstream
J	7-9	Close Downstream
K	10-12	Far Downstream

Cases E, F, I, and J use gauges close the buoy and are expected to contain more information regarding radiation than the gauges farther from the buoy, D, G, H, and K. The cases with downstream gauges, F, G, J, and K are expected to contain beach reflections and will provide insight into the importance of using this information in acceleration prediction.

The purpose of these test cases are to examine the individual contributions of each

Figure 4.6: Illustration of the wave gauges used for the cases described in Table 4.3 where waves propogate from left-to-right.

gauge group to network accuracy. Each group consists of three wave gauges, but the effect of using only a single gauge from the same group will also be investigated. In section 4.4, gauge quantity will be explored, and these tests will be re-used to compare the performance from a single, versus triple wave gauge predictor.

4.2.2 Results

One trend demonstrated by the results, as shown in Figure 4.7 was that wave speed has less of an impact on performance than gauge placement. The group that the input gauges belong to reflects in the RMSE regardless of wave speed.

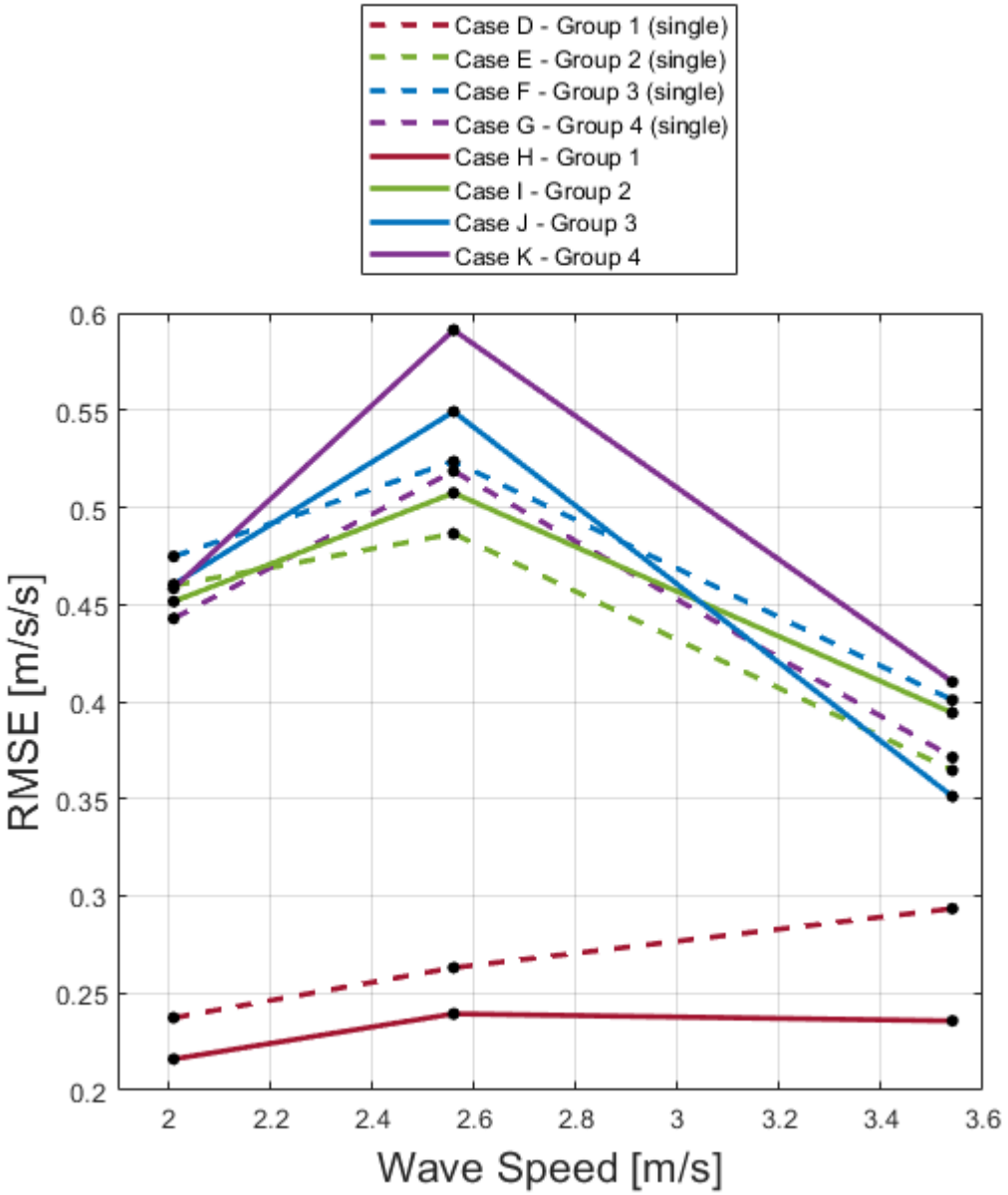

Figure 4.7: The resulting RMSE for cases D through K from Table 4.3, demonstrating a significant favorability of Gauge Group 1.

The cases belonging to group 1, (case D, and case H) had the lowest RMSE of all cases, indicating a higher network performance. The downstream cases, and the cases from group 2 performed at comparable levels to one another. In the cases consisting

of gauges from group 2, (case E, and Case I), poor network performance can likely be attributed to the lack of distance between the measurement and the buoy, which provides very little warning before the wave arrives at the site of the buoy.

As expected from the results of the upstream/downstream test cases, the cases consisting of downstream gauges, (F, G, J and K) did not perform well. This is due to the measurements being taken behind the buoy; only to receive information after the buoy has already responded to the incoming wave.

Another noteworthy observation on this plot is that the triple-gauge test cases often performed better than their respective single-gauge cases. This can be seen as the dotted(single-gauge) and dashed(triple-gauge) lines of the same color. This trend is less prominent for groups 2, 3 and 4, but is quite noticeable in the cases belonging to group 1. This provides insight to the future gauge quantity tests, and will be revisited in section 4.4.

4.3 Wave Gauge Topology

Nine cases, described in Table 4.4 and illustrated in Figure 4.6, were created to understand the impact of wave gauge shape on acceleration prediction. After a description

of the shapes, the results of trained neural networks are provided along with a summary of the important factors.

4.3.1 Case Descriptions

The shapes investigated include triangles of different types, size, and orientation. A diamond pattern and two straight line cases were also considered. In Table 4.4 the "Sourrounded" location means that the bouy was inside the set of wave gauges. The size designations of "Small" and "Large" for the traingle shapes are relative to the other shapes in that category.

Table 4.4
Cases used to evaluate the effect of wave gauge topology on acceleration prediction with abbreviations: T=traingle, D=diamond, L=line.

Case #	Gauge #s,	Shape	Size	Location	Direction
L	5,7,9	T	Small	Surounded	Forward-Facing
M	2,7,9	T	Large	Surounded	Forward-Facing
N	2,4,6	T	Small	Upstream	Forward-Facing
O	4,6,8	T	Small	Surounded	Backward-Facing
P	4,6,11	T	Large	Surounded	Backward-Facing
Q	1,3,5	T	Small	Upstream	Backward-Facing
R	2,4,6,8	D	N/A	Sourounded	N/A
S	2,5	L	N/A	Upstream	N/A
T	2,5,8,11	L	N/A	Sourounded	N/A

One important detail about this test set is that while 6 of these cases had access only to 3 gauge measurements, 3 of them had access to a slightly different number of

Figure 4.8: Illustration of the wave gauges used for the cases described in Table 4.4.

gauges. This will be considered when observing the results, as there may be a slight change in bias toward these cases. These cases will be re-examined in a different light later in Section 4.4 when gauge quantity is discussed. For this section, the pattern of the gauge layout is what will be prioritized when finding the network performance.

4.3.2 Results

There were visible distinctions between high, moderate, and low performing cases. The results for the topology cases described in Table 4.4 are shown in Figure 4.9.

Red = Upstream; Blue = Surrounded; Green = Large Shape;

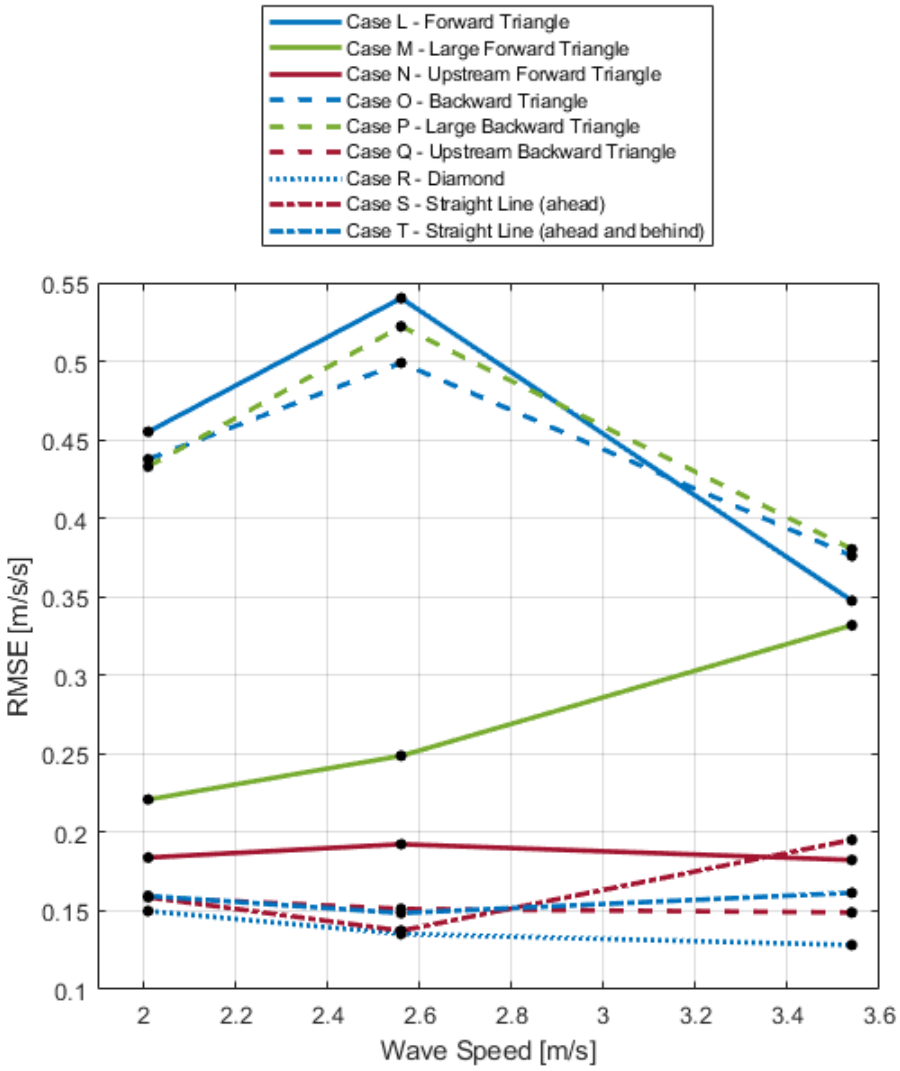

Figure 4.9: The resulting RMSE from the gauge Topology Cases in table 4.4, where the diamond case appears to be preferred.

Solid Lines = Forward-Facing Triangle; Dashed Lines = Backward Facing Triangle;

Dotted Line = Diamond Shape; Dash-Dotted Line = Straight Line Formation.

For each black dot, a neural network was trained and the performance evaluated.

Examining each color will show each case as either upstream, a surrounding layout, or an augmented shape. Solid lines indicate the shape is a forward facing triangle, and the dashed lines indicate backward facing triangles. Similarly, a dotted line is coincident with a diamond pattern, (including 4 gauges), and the dash-dotted line is indicative of a straight line formation (either 2, or 4 gauges).

The red lines on figure 4.9 indicate upstream data, regardless of shape. All 3 upstream test cases were among the top performers, as expected from the previous results section. The 'Large' shaped cases, (case M and P: the large triangle shapes) were not as consistent. Case M performed in the moderate range, while case P was the worst case of all. Using conclusions from the previous sections, it is likely that case M outperformed case P by virtue of having even only a single gauge in group 1. This demonstrates the benefit of having gauges at a further distance, as the lower performing case P even has two gauges upstream of the buoy, only at a much closer range. Therefore, it can be concluded that using fewer gauges at a far distance upstream is more beneficial than using multiple gauges closer to the buoy.

The blue lines indicate a formation that surrounds the site of the buoy, using both upstream and downstream gauges. Among those is the highest performing case: case R. This was the diamond case with 4 gauges. However, the next-best performing case to the diamond shape is the 2-gauge straight line upstream formation. This demonstrates a priority of gauge placement over gauge quantity once again, however,

a clear benefit to an increased number of gauges in the acceleration predictor is observed. This will be verified in the subsequent section.

4.4 Wave Gauge Quantity

Another critical factor to consider is the quantity of gauges; specifically, to find if there are diminishing returns from adding more gauge measurements as inputs. It has been shown in the previous sections that a higher number of gauges is often associated with increased performance. It is often recommended to use a significant amount of data during the training of a network, and therefore, having more inputs in general may prove to be more helpful for predicting buoy motion. This portion of the study is dedicated to determining whether fewer gauges can be used with a similar success rate. This will be done using selections from the previous test cases to observe the direct relationship between gauge quantity and network performance. It is anticipated that more gauges included in the acceleration predictor will provide a better result.

4.4.1 Case Descriptions

Using the previous test cases and sorting them via gauge quantity, only the previously top performing case of each quantity will be considered. Table 4.5 sorts these previous cases based on the number of gauges they include.

Table 4.5
Cases used to evaluate the effect of including more, or less input gauges.

# Gauges	Case	Shape
1	D	Group 1 (Single)
2	S	Straight Line (Ahead)
3	H	Group 1
4	R	Diamond
6	A	Groups 1 and 2
12	C	All Gauges

The same waveforms from table 4.2 will be also be used for this section.

4.4.2 Results

Figure 4.10 demonstrates the RMSE of these cases, observing gauge quantity only.

This set of cases provided a different result than previously anticipated. The top performing case continued to be case R, the diamond shape. This case only has four gauges, which indicates that gauge quantity is still less important than arrangement

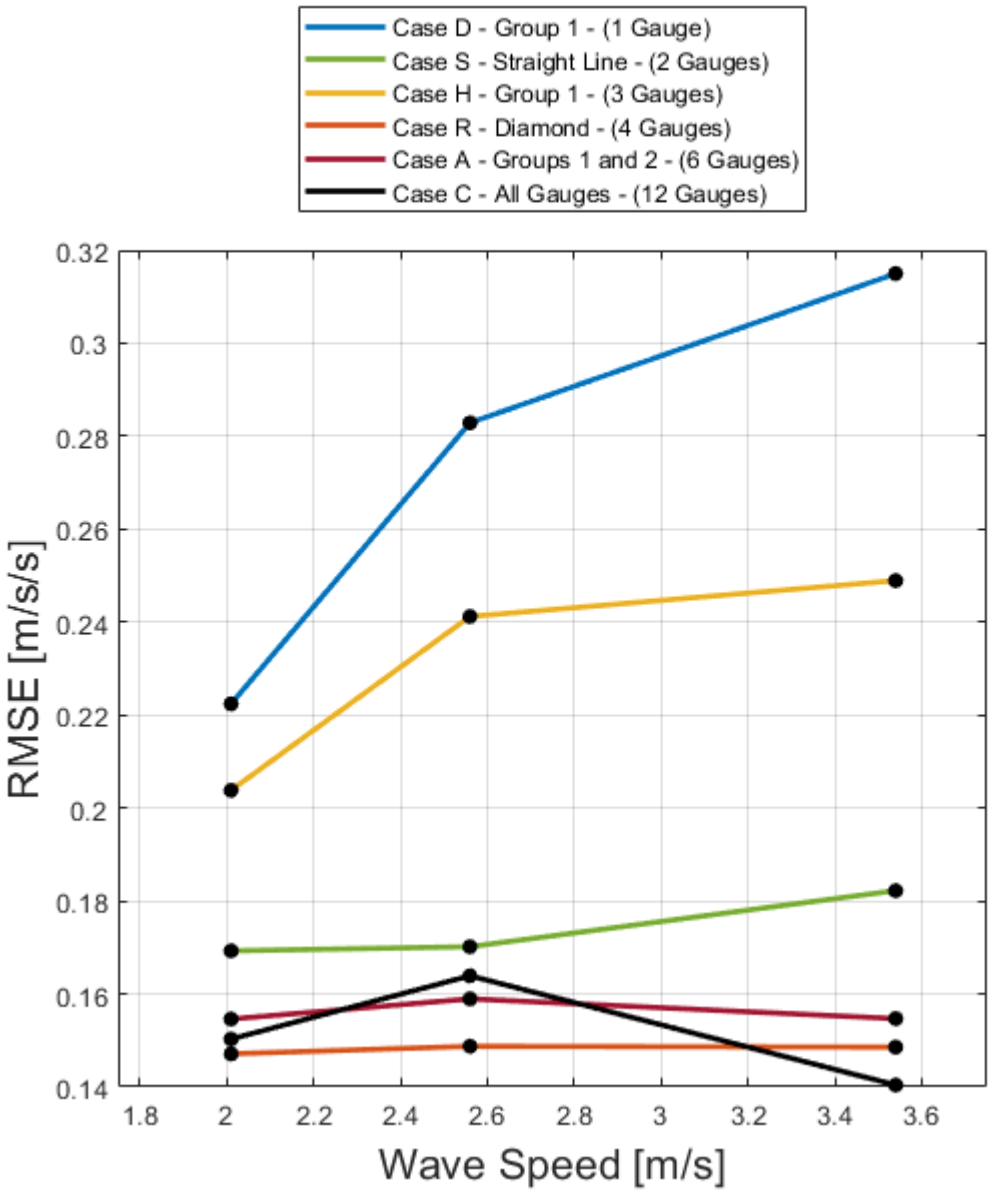

Figure 4.10: The resulting RMSE from the gauge quantity cases in table 4.5.

and placement. The cases that were anticipated to succeed came in closely behind, including case C (12 gauges) and A (6 gauges).

Although gauge quantity has proven to be of less value than placement, it should not be overlooked. Case D consists of a single gauge from group 1. Regardless of using a critically placed gauge in the front row, the lack of measurements is detrimental to the network performance. Cases S and H include 2 and 3 gauges of high-value placement, yet they still fail to meet the standard set by cases R, A and C. This observation indicates that although gauge placement may be more critical than gauge quantity, at least 4 well-placed gauges may need to be used in the predictor to promote a higher-performing network.

4.5 Acceleration as a Network Input

In many applications, acceleration can be easily measured and is readily available. If this is the case, it could help the network tremendously during operation to receive real-time measurements of buoy acceleration to predict buoy acceleration t_H seconds into the future. To observe the benefit of streaming current acceleration data as an additional input, the top performing cases will be re-visited to also include acceleration(t) as an input. It is likely that by providing the target in real time, the network response can be greatly improved.

4.5.1 Case Descriptions

Using the same cases from previous section, these test cases will now be investigated both with, and without acceleration as an additional input to quantify network performance. It is anticipated that even the lower performing cases will significantly improve in network performance when allowed to stream current acceleration measurements.

Table 4.6
Cases used to explore the effect of including current acceleration measurements as a network input, sorted by gauge quantity.

Case	# Gauges	Including $\ddot{\zeta}$
D	1	D_a
S	2	S_a
H	3	H_a
R	4	R_a
A	6	A_a
C	12	C_a

4.5.2 Results

The results shown in Figure 4.11 demonstrate a conditional relationship between the inclusion of acceleration and the performance of the network. In the figure, the cases of the same type (with, or without acceleration) are included as lines of the same color. Solid lines indicate cases without acceleration, and dashed lines indicate cases that

do include acceleration in the predictor. Figure 4.11 shows evidence that including

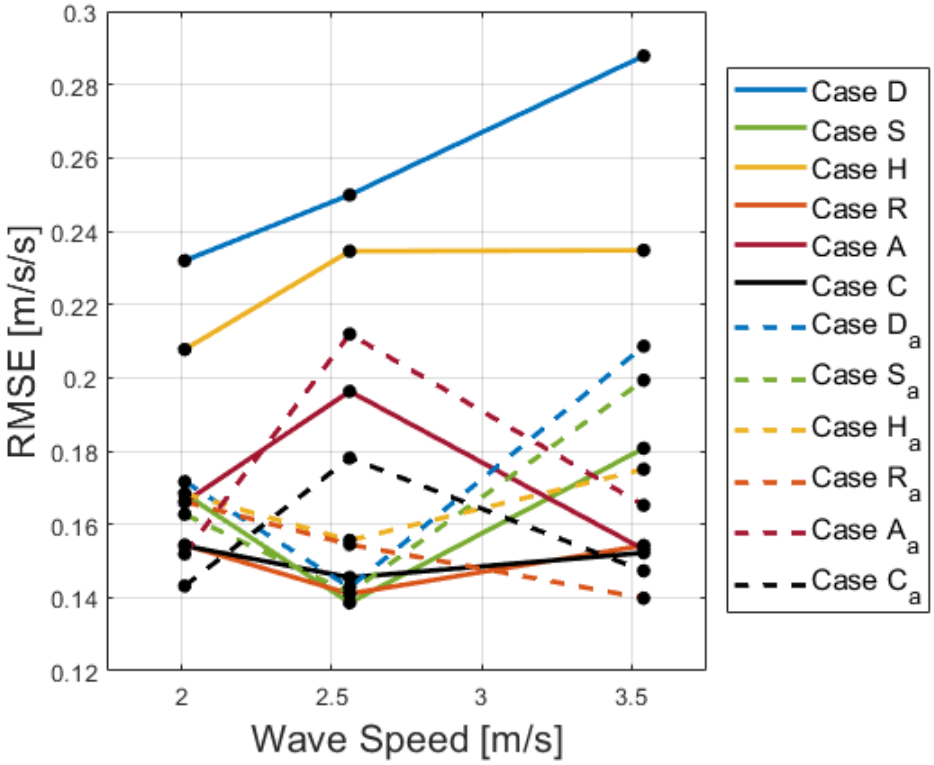

Figure 4.11: The resulting RMSE from re-running the gauge quantity cases, including those with the added accleration input in table 4.6.

acceleration can help in most cases, most noteably the cases with less gauges, such as cases D, H and R. These cases appeared to halve the error that occurred in gauge-only form. As the number of gauges increases, such as in case A where there are 6 gauges included in the acceleration predictor, and case C that includes 12 gauges, the returns diminish, and could even harm the performance. Case C demonstrates a case where the performance was routinely worsened upon including acceleration as an input. For most cases, the inclusion of acceleration in real-time could be added

to a set of gauges to improve performance. Acceleration could also be added in the event that not many gauges are available, and its inclusion might make up for this loss of information.

4.6 The Number of Backvalues and the Forecast Horizon

When handling neural networks, it is often necessary to use several back values to allow the network access only to the most relevant information. The number of back values N_B is directly related to the duration of time t_B that the network can access to make an estimation. t_B is the product of the number of back values and the time step Δt between measurements.

$$t_B = N_B \Delta t$$

The forecast horizon t_H is the amount of time in the future that the network is being trained to predict. N_H is the number of time steps into the future the network will be trained to predict.

$$t_H = N_H \Delta t$$

4.6.1 Case Descriptions

To determine how the number of back values and forecast horizon may be related, networks will be trained based on different ratios for $\frac{N_H}{N_B}$. If this ratio is near 1, it is anticipated that the trained network will perform its best. If this ratio is greater than 1, then there is a longer forecast horizon than duration of back values given to the network for a prediction. If this ratio is less than 1, then that means there is an excess of back values and a brief forecast horizon. It is hypothesized that for cases with a ratio that is far greater than 1, the network will perform poorly as it is being asked to make predictions further out than what is provided to make the prediction. Shown below in Table 4.7 are the test cases that will be performed to quantify this metric.

To provide a more diverse representation of waveforms, a new test set will be used for this section, shown in Table 4.9. These waveforms still have slow, medium and fast classifications, but will be used to provide a different sample set.

4.6.2 Results

Both of the test sets from Table 4.7 and Table 4.8 provide an indication that the ratio between the forecast horizon and number of backvalues is indeed relevant to

Table 4.7
Parameters that will be modified to analyze network performance with a $\frac{N_H}{N_B}$ that is greater than 1.

N_H	t_H, (sec)	N_B	$\frac{N_H}{N_B}$
5	0.25	5	1
10	0.50	5	2
15	0.75	5	3
20	1.00	5	4
25	1.25	5	5
30	1.50	5	6
35	1.75	5	7
40	2.00	5	8
45	2.25	5	9
50	2.50	5	10
55	2.75	5	11
60	3.00	5	12
65	3.25	5	13
70	3.50	5	14
75	3.75	5	15
80	4.00	5	16

network performance.

Table 4.7 demonstrated the resulting RMSE when $\frac{N_H}{N_B}$ is greater than 1. This demonstrates the performance as the forecast horizon N_H exceeds the number of backvalues N_B. As anticipated, the performance as $\frac{N_H}{N_B}$ grows greater than 1 only gets worse. This is because there are more forecast horizon time-steps than backvalues for those scenarios.

In addition, wave speed did prove to be a factor in determining the RMSE for each case. Waveform 2 is the slowest, and as a result, it appears to have the lowest error.

Table 4.8
Parameters that will be modified to analyze network performance given a $\frac{N_H}{N_B}$ ratio that is less than 1.

N_H	t_H	N_B	$\frac{N_H}{N_B}$
10	0.5	1	0.1
10	0.5	2	0.2
10	0.5	3	0.3
10	0.5	4	0.4
10	0.5	5	0.5
10	0.5	6	0.6
10	0.5	7	0.7
10	0.5	8	0.8
10	0.5	9	0.9
10	0.5	10	1.0

Table 4.9
The new waveform test set that will be used for this portion of the study.

Waveform #	$c_{1/3}$, m/s	Classification
2	2.03	S
4	2.52	M
7	3.39	F

This error increases with the speed of the incoming wave, as waveforms 4 and 7 prove to have a substantially higher error. This phenomenon is also concurrent with the results in Figure 4.12.

Figure 4.13 demonstrates how the results are consistent when the ratio is less than 1. This is likely due to the fact that there are always more back values than indices in the forecast horizon, so an adequate amount of information is always available for any given prediction on the forecast horizon. Slower waveforms demonstrate less error,

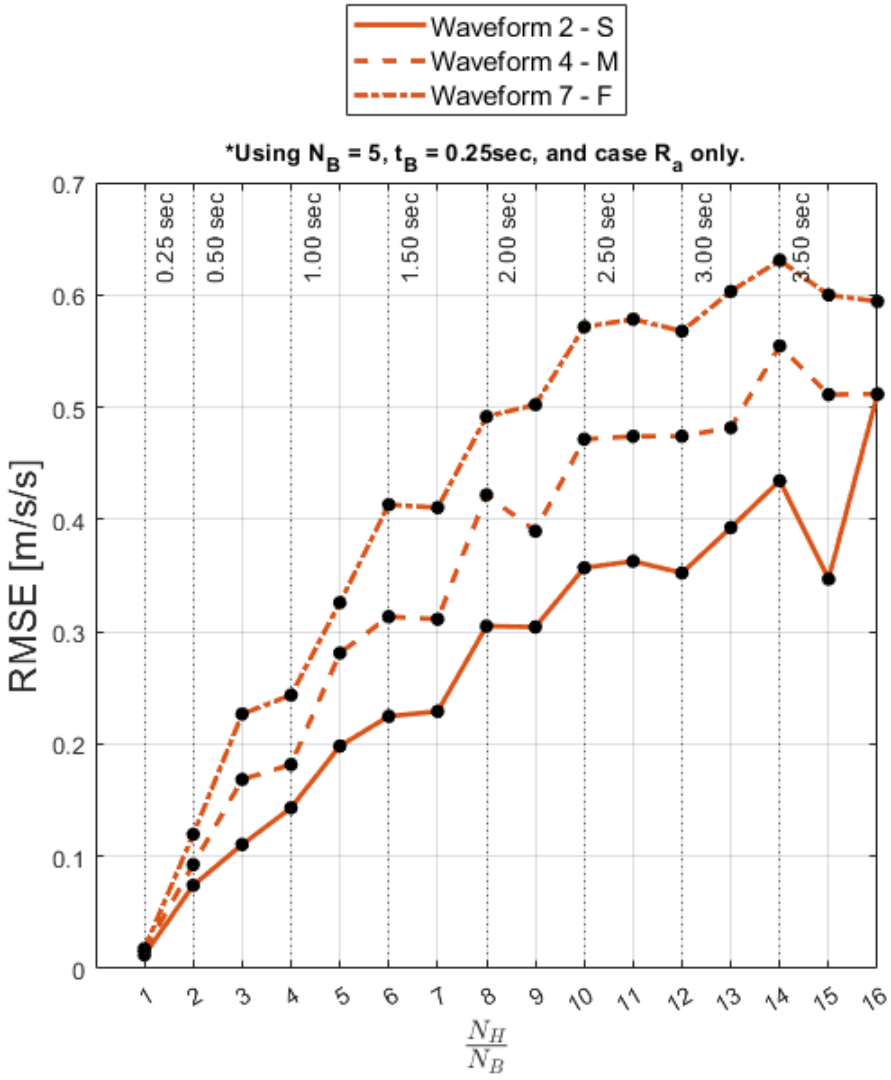

Figure 4.12: The resulting RMSE from using the data in table 4.7

whereas faster waveforms demonstrate more error.

These results demonstrate the fact that increased wave speeds do have an impact on network performance. These results also suggest that the ideal ratio for forecast horizon to the number of backvalues $\frac{N_H}{N_B}$ is somewhere near, or below 1.

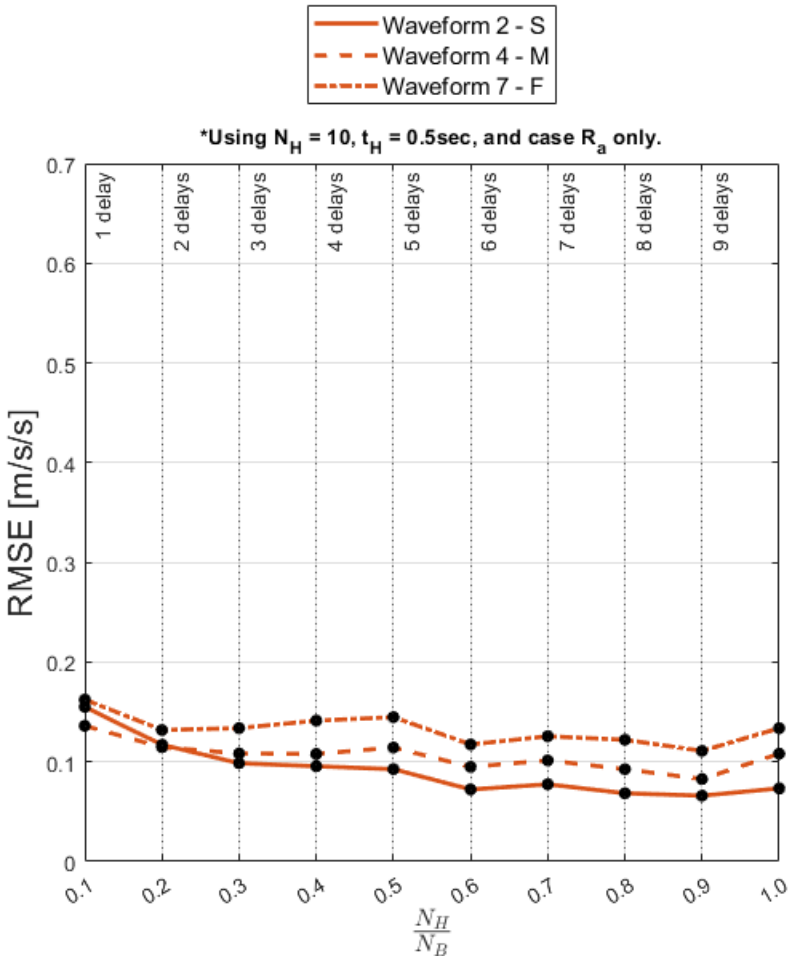

Figure 4.13: Illustration of the wave gauges used for the cases described in Table 4.8

4.7 Waveform Complexity

As mentioned previously, depending on the composite number of frequencies used to make a waveform, it is anticipated that those waveforms with higher numbers of dominant frequencies will be harder for the network to track. For example, for

a single-frequency waveform, it is simple to be able to predict what the value may be at a given point in time using a mathematical approach. When there are many dominant frequencies and an offset by a phase shift, waveform patterns can suddenly become more difficult to anticipate, especially for large motion. It is hoped that the network will be able to track buoy motion both for simple and complex waveforms when given a reasonable training set. By extensively training a neural network for a variety of waveforms, it might be possible to avoid the need for expensive traditional computational methods and find one solution for many waveforms, while also providing a more accurate estimation.

Like the other test cases, this aspect will be observed by ranking the average root mean square error of the network performance. In the following section, the figures will give insight on how the network responds to testing on 'simple' or more 'complex' data.

4.7.1 Case Descriptions

For this factor, waveforms with 1, to 5 dominant frequencies were considered. Table 4.10 shows which waveforms were selected for this purpose. Because the algorithm has been built to use 7 waveforms as a training set and 3 waveforms for the test set to provide enough data for the predictor, these 5 tests will come from various trained

Table 4.10
Waveforms used to evaluate network performance when tested on waveforms of varying complexity.

n	Waveform #
1	8
2	10
3	3
4	5
5	2

networks.

These test sets were trained for a forecast horizon of 1 second, and 20 backvalues, for a $\frac{N_H}{N_B}$ ratio of 1, as deemed appropriate in the preceeding section.

4.7.2 Results

The results based on wave complexity are shown in Figure 4.14 Upon performing this test, one thing became evident; as the number of waveforms increase, the error seems to be reduced contrary to what was expected. This could be attributed to the lack of additional single-frequency waveforms beyond waveform 8 used for this test. When this waveform is used for testing, it cannot also be used for training, and thus the network had not yet been exposed to this kind of wave. This poor performance may be improved if more simple waveforms were introduced to the training set.

Another observation is that each test case performed within a similar range. Case C that included all 12 gauges appeared to be a poor performer when compared to the others, until more complex waveforms were tested. Cases R_a and D_a performed similarly to one another, regardless of case D_a having only a single gauge from row 1. This shows that with the appropriate number of backvalues, it is possible to achieve a fairly uniform response regardless of the number of gauges used and the complexity of the incoming waveform.

It is expected that if more complex waveforms are tested, the error will eventually plateau, and provide consistent results, hopefully in favor of a lower error. Ultimately, this will only be discovered in an extended study where a greater diversity of waveforms are used, including more than just a single regular wave.

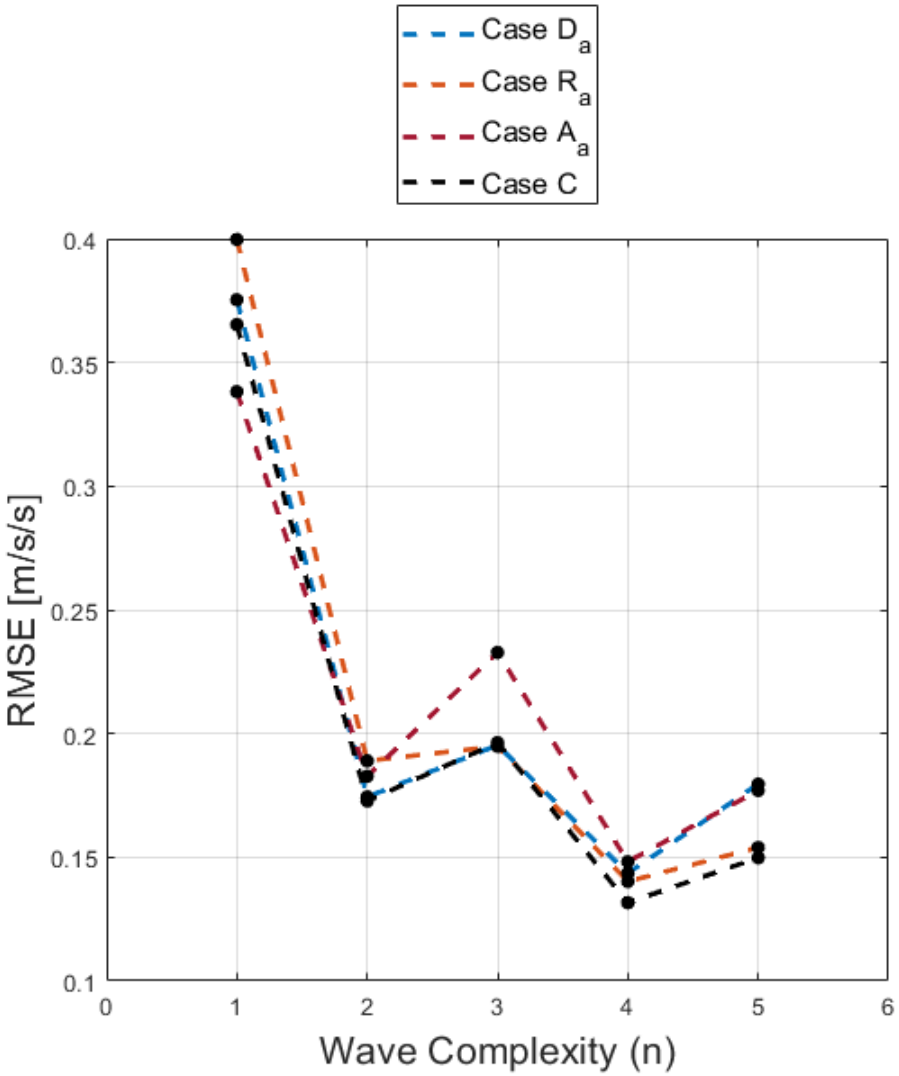

Figure 4.14: Illustration of the the cases described in Table 4.10 suggesting improvement when tested on a higher number of frequencies.

Chapter 5

Conclusions

This chapter contains the summary of the findings of this work as well as a conclusion and possible future work.

5.1 Summary

The intention of this work was to characterize the factors that influence the success of an accleration predictor. These factors included the effect of upstream and downstream measurements, gauge placement relative to wave speed, the layout and shape of the gauges, the quantity of gauges, the effect of including acceleration as an input, and the effect of testing on more, or less complex waveforms.

5.2 Conclusions

Through the investigation of these factors, it was evident that there was a preference for the use of gauges further upstream. As a result the downstream gauges, especially when used alone, provided significant error. Downstream gauges are most effectively used in conjunction with upstream gauges to get a complete view of the wave tank. When using wave gauges as part of the acceleration predictor, it is recommended to use a minimal amount in the downstream region, perhaps only a single gauge, as too many can provide misleading information to the network. Due to the nature of upstream gauges, and how they observe the wave elevation before it reaches the buoy, upstream gauges are recommended to be the first line of defense for this type of problem.

The findings in relation to wave speed and gauge placement seemed to validate the findings from the upstream and downstream cases. Upstream gauges, regardless of wave speed, still proved to be more effective at predicting future buoy acceleration. Similarly, gauges that were too close to the buoy performed just as poorly as the gauges from the downstream region. This reaffirms our recommemendation of the use of gauges significantly upstream from the buoy to predict acceleration.

In regard to gauge layout and topology, the largest factor appeared to be whether

or not there was at least one gauge in the furthest upstream row. However, the most successful shape appeared to be the diamond shape, likely due to being a fully-surrounding shape, and including one gauge far upstream, two gauges immediately upstream, and one gauge in the rear.

The quantity of wave gauges for the acceleration predictor was anticipated to be one of the largest factors. However, it appears that similar, if not better results can come from more strategic placement of gauges, rather than sheer quantity. This was evident as the diamond case with 4 gauges surpassed the case with all 12 gauges. It is our recommendation that when designing the accleration predictor and choosing the network inputs, a surrounding shape that includes gauges far upstream is used. The findings of this study indicate that a full fine-grid of wave gauges is not required. It appears that a similar level of performance can be achieved with fewer gauges, so long as they are properly placed.

The effect of using the buoy's instantaneous acceleration seemed to behave as expected. When including this measurement in the accleration predictor, most cases seemed to improve. However, this effect was more substantial in cases where there are only a few gauges, such as in single-gauge cases. When including accleration in the acceleration predictor, more information about the buoy's behavior is provided, and thus similar results can be achieved as compared to cases with a higher number

of gauges. It is recommended that if only a few gauges are present in the acceleration predictor that an additional input of instantaneous buoy acceleration is used to achieve a similar result to a fine grid of gauges. This could perhaps make the experiemntal setup easier, cheaper, and also more accurate. One consideration about including buoy acceleration was that it appeared to make the case with a higher number of wave gauges decrease in performance. Therefore, acceleration should be used to enhance cases with only a few gauges, instead of being added to a fine grid of gauges.

The relationship between forecast horizon and the number of backvalues seemed to behave as expected. When determining the number of backvalues necessary, the largest aspect to consider appeared to be the forecast horizon. It is recommended that a ratio close to $\frac{N_H}{N_B} = 1$ is used. When this ratio exceeded 1, the error grew substantially, and similarly, when this ratio was less than 1, the error also grew. To achieve an acceptable performance from the network, it is important to provide the proper number of backvalues relative to the forecast horizon.

Wave complexity proved to be less impactful than anticipated. In fact, waveforms with a higher number of dominant frequencies performed better than those with fewer frequencies. This could be due to the lack of sufficient single and double frequency waveforms that were created for this study. Because there was only one

single-frequency waveform included in this study, it could only either be used in testing or in training. Therefore, this study demonstrated poor performance for this case.

5.3 Future Work

For future work and further exploration of this subject, perhaps a gauge group even further upstream may prove to be beneficial to the acceleration predictor. Gauge distance relative to the buoy in this study seemed to improve the acceleration predictor substantially, however, it could be important to determine if there are diminishing returns, or even destructive qualities of including gauges too far upstream.

It is also recommended that future work includes a higher number of waveforms with sufficient diversity in complexity to determine the true cause for poor performance on single-frequency waveforms.

References

[1] "Wave Gauges", Edinburgh Designs. Accessed: April 26, 2024. [Online]. Available: http://www4.edesign.co.uk/product/wavegauges/.

[2] B. Guo, R. Patton, and S. Jin, *Identification and Validation of Excitation Force for a Heaving Point Absorber Wave Energy Convertor*. 2017.

[3] R. Genest and J. Ringwood, "Receding horizon pseudospectral optimal control for wave energy conversion," *2016 UKACC 11th International Conference on Control*, pp. 1–6, 2016.

[4] G. Giorgi and J.V.Ringwood, "Computationally efficient nonlinear froude-Krylov force Calculations for heaving axisymmetric wave energy point aborbers," *Journal of Ocean Engineering and Marine Energy*, vol. 3, 2016.

[5] J. F. J. Hals and T. Moan, "Constrained Optimal control of a heaving buoy wave-energy converter," *Journal of Offshore Mechanics and Arctic Engineering*, vol. 133, 2010.

[6] E. N. K. Mahmoodi and A. Razminia, "Wave excitation force forecasting using neural networks," *Energy*, vol. 247, 2022.

[7] T. H. Havelock, "Waves due to a floating sphere making periodic heaving oscillations," *Royal Society*, vol. 231, 1955.

Appendix A

Collection of Waveforms

Shown in Table A.1 is the composition of each of the 10 waveforms used for this study. These waveforms were created from a composition of one or multiple sine waves of various frequencies and amplitudes. Some of these waveforms also have a phase shift applied. The entries for each waveform are listed in ascending order based on the composite frequencies. The amplitudes and phase shift information is listed in the same respective order.

This section also provides a visual representation of each waveform. These waveforms are shown in A.1 through A.10. For all of these figures, the upper plot demonstrates wave elevation measurements from the centermost gauge in group 1 (furthest upstream group), and the bottom plot shows the corresponding buoy position response.

Table A.1
Waveform composition in greater detail, as generated from Edinburgh Designs Wave Synthesis Software.

#	Frequencies, Hz,	Amplitudes, m	Phase Shift, rad
1	0.50 0.70, 0.80, 0.90, 1.00	0.05, 0.05, 0.05, 0.05, 0.05	0, 2, 0.6, 0, 0
2	0.20, 0.55, 0.75, 0.80, 0.85	0.0175, 0.025, 0.03, 0.035, 0.015	0, 4, 0, 3, 1.25
3	0.50, 0.70, 1.00	0.05, 0.075, 0.05	0, 2, 1
4	0.20, 0.55, 0.80, 1.00	0.02, 0.03, 0.04, 0.02	0, 4, 3, 1
5	0.40, 0.60, 0.75, 1.00	0.03, 0.05, 0.04, 0.02	0, 3.60, 0, 3
6	0.50, 0.60	0.05, 0.075	0, 2.80
7	0.40, 0.50, 0.86	0.035, 0.05, 0.02	0.20, 2.5, 2
8	0.45	0.09	0
9	0.40 0.50, 0.90	0.04, 0.05, 0.04	1.50, 0, 1.50
10	0.40, 1.00	0.05, 0.02	0, 1.50

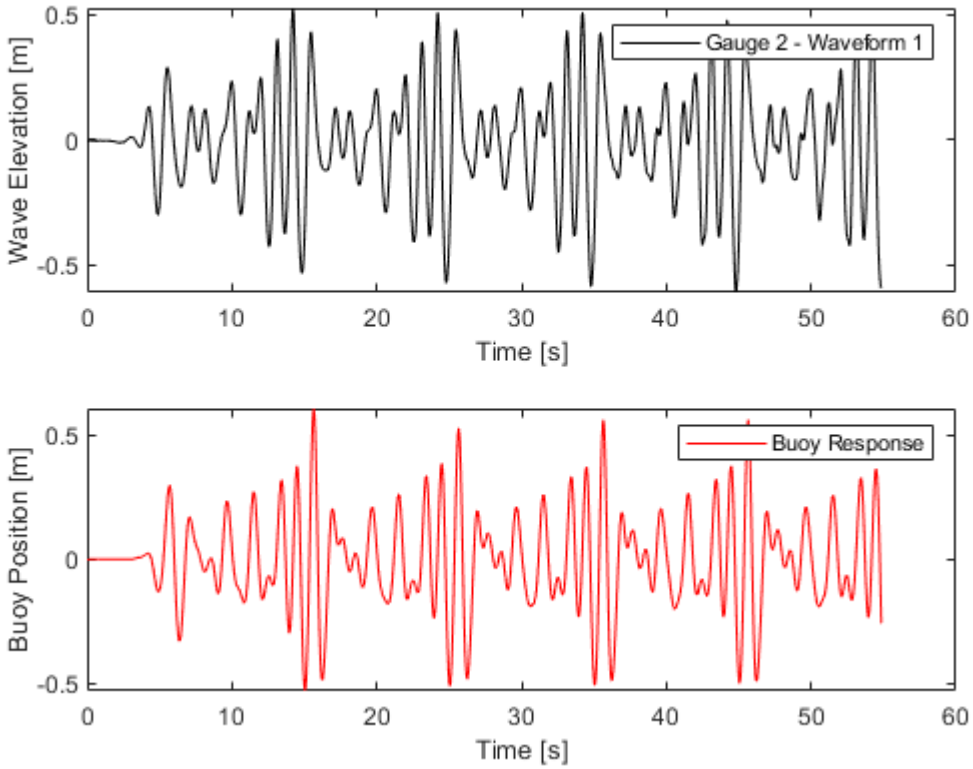

Figure A.1: Wave elevation and buoy response for waveform 1.

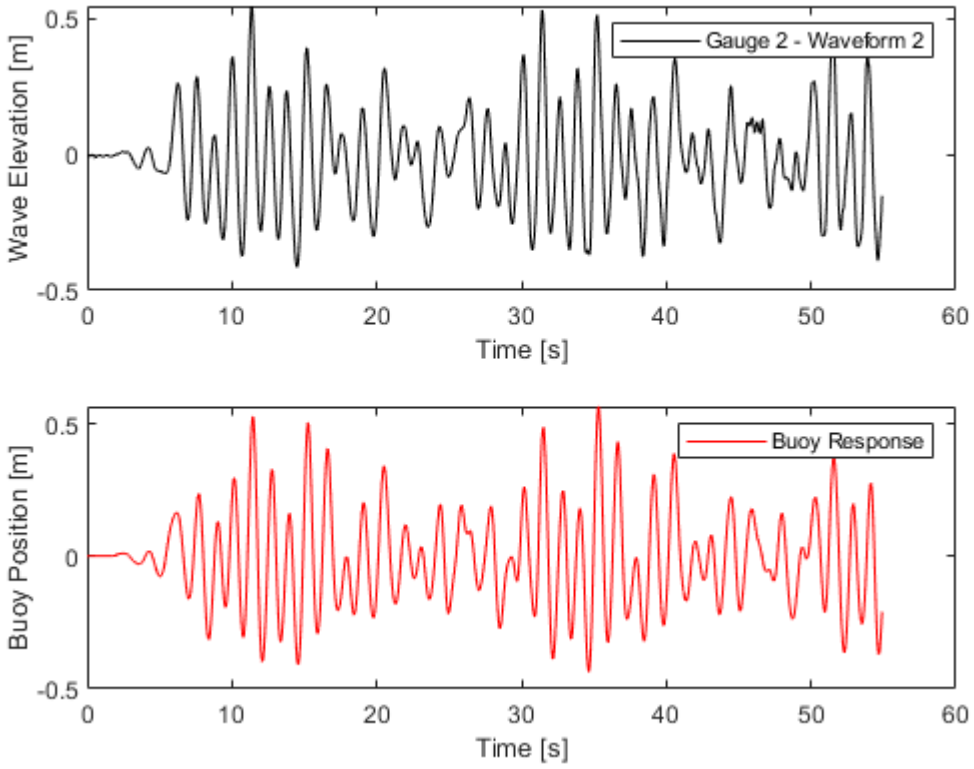

Figure A.2: Wave elevation and buoy response for waveform 2.

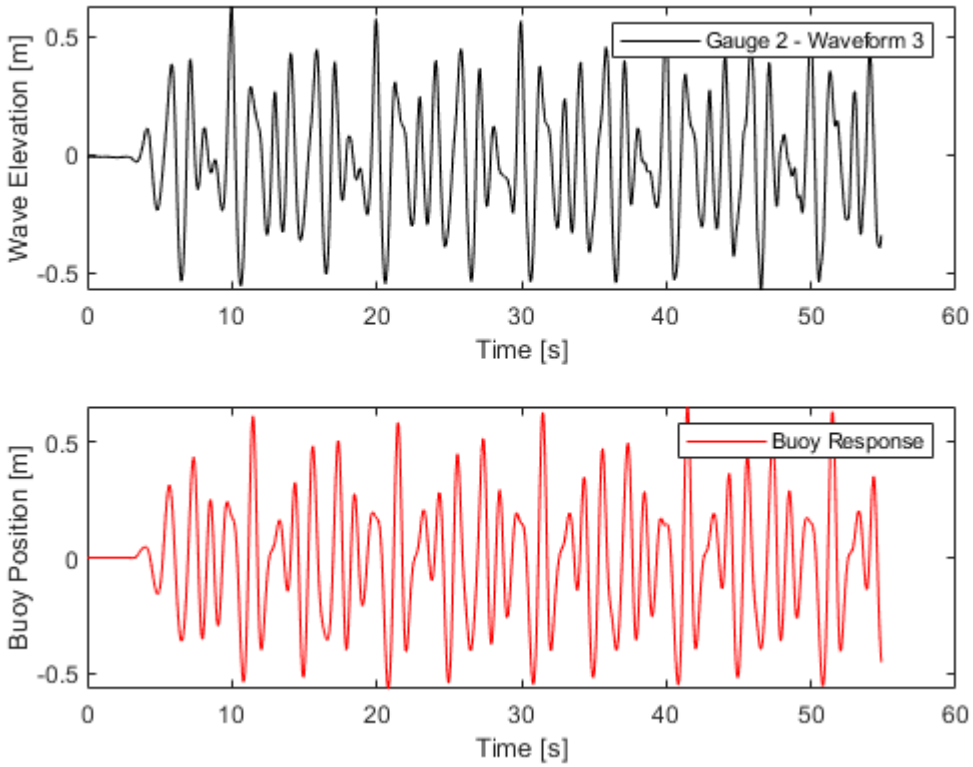

Figure A.3: Wave elevation and buoy response for waveform 3.

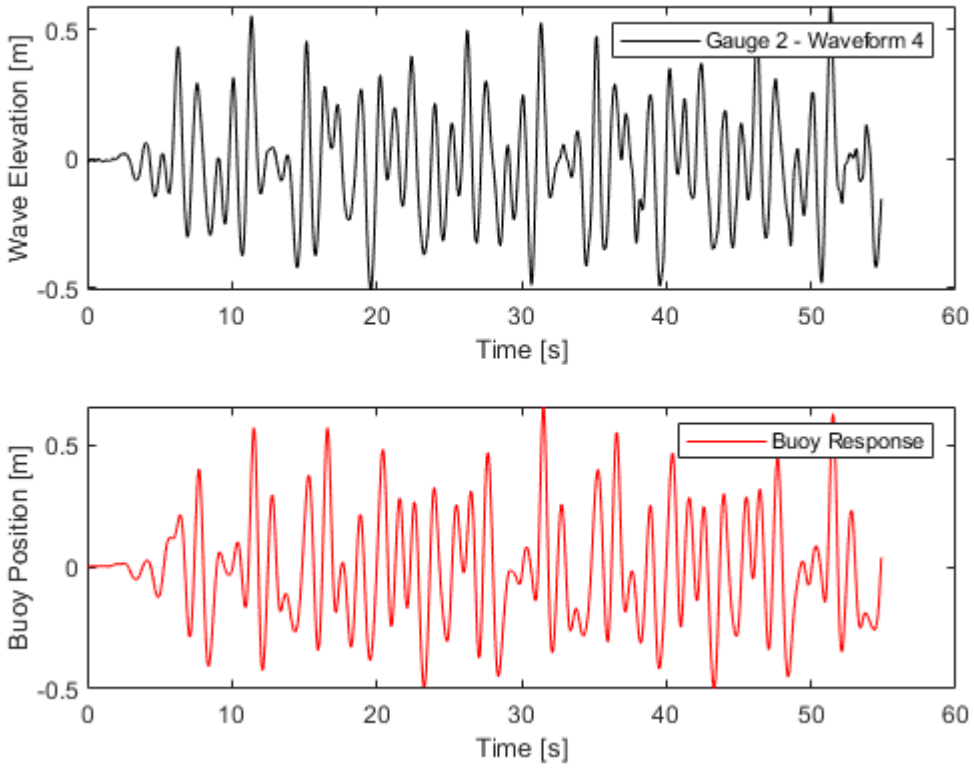

Figure A.4: Wave elevation and buoy response for waveform 4.

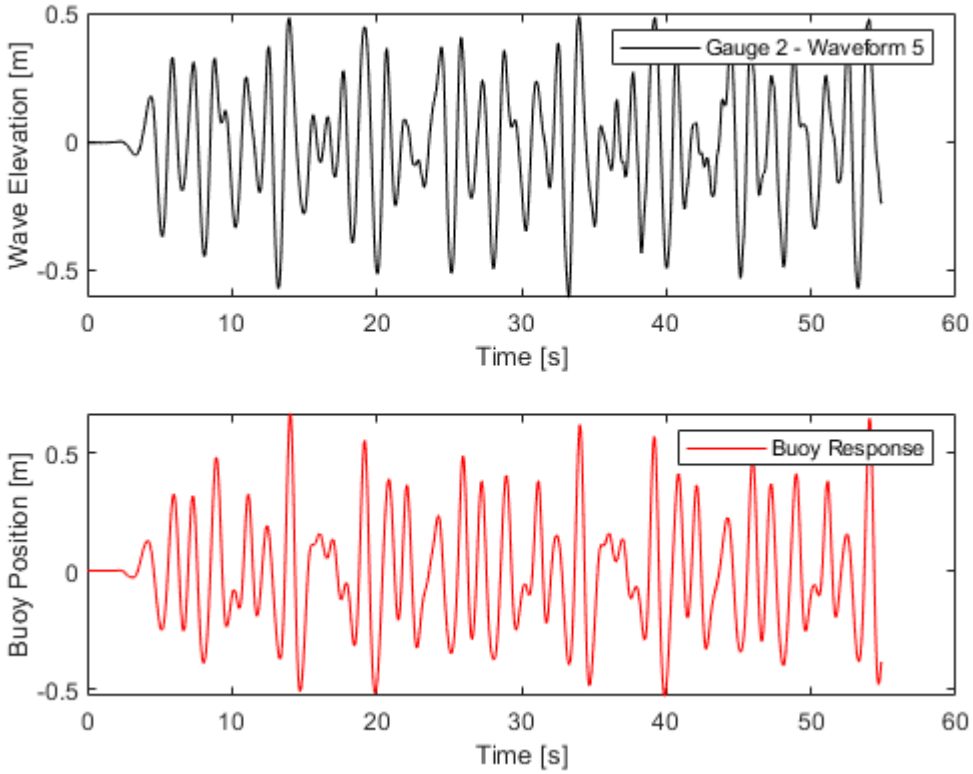

Figure A.5: Wave elevation and buoy response for waveform 5.

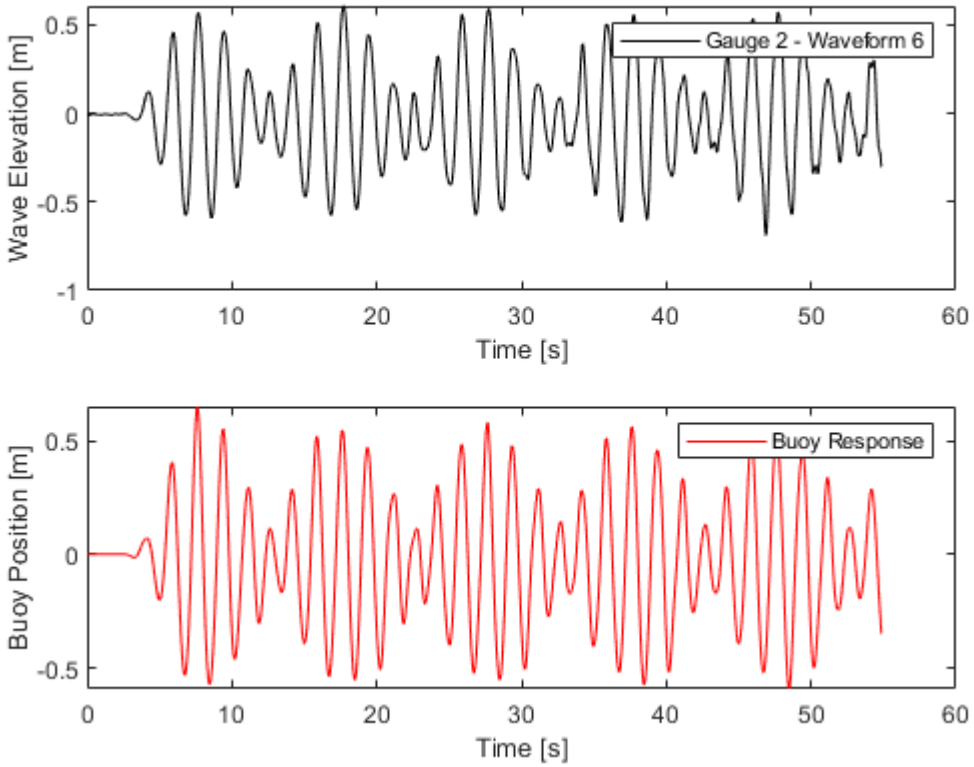

Figure A.6: Wave elevation and buoy response for waveform 6.

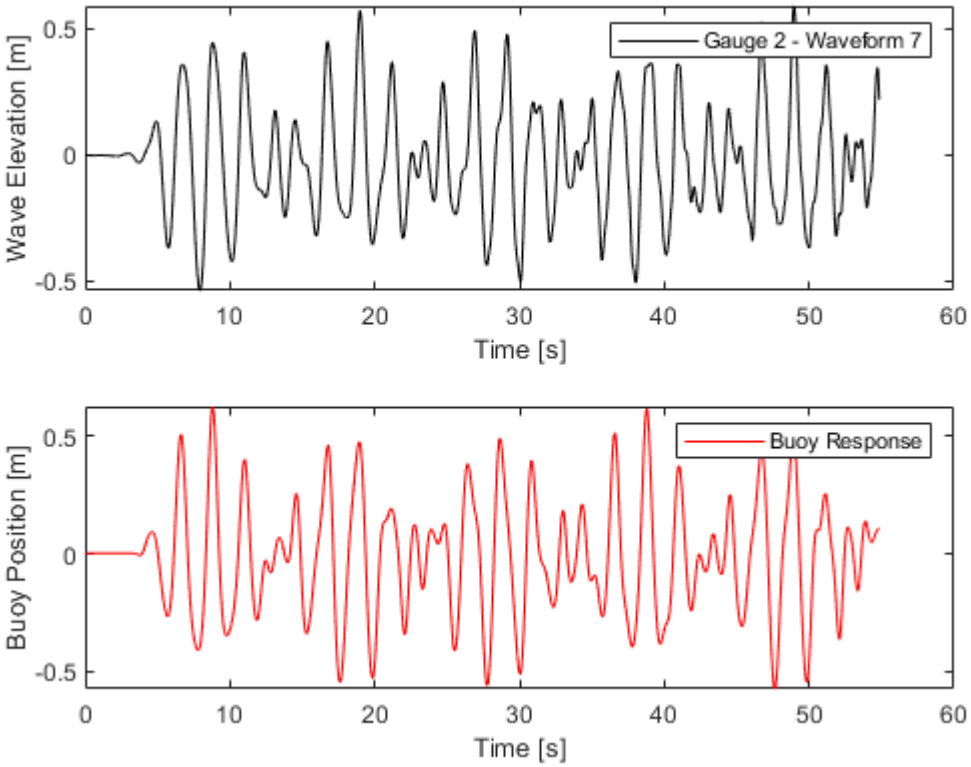

Figure A.7: Wave elevation and buoy response for waveform 7.

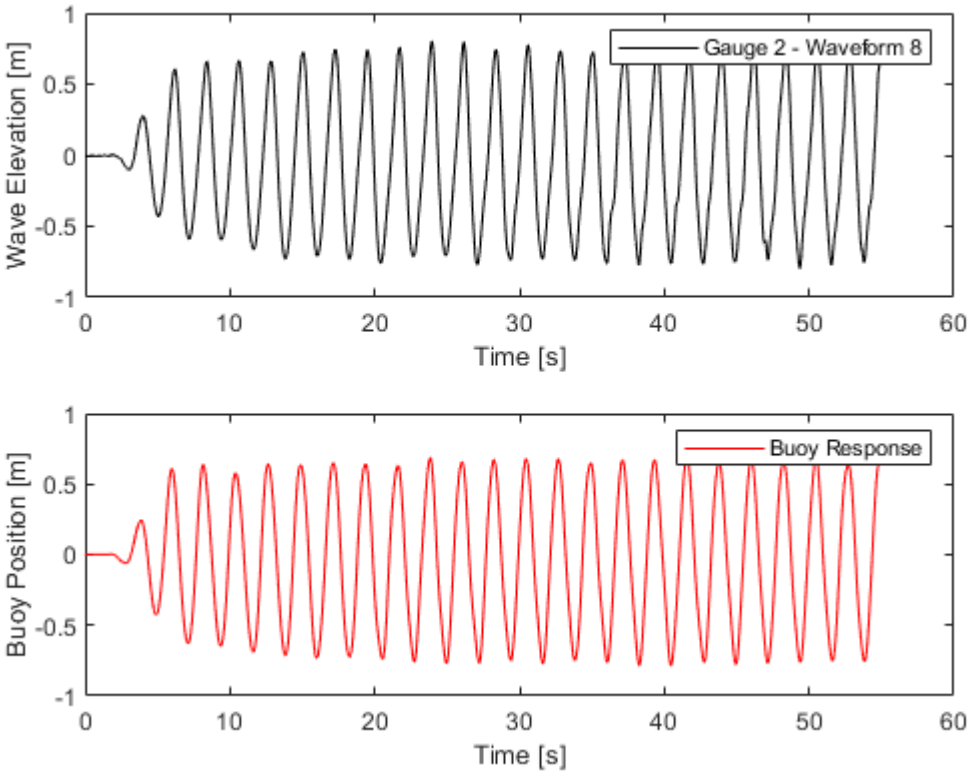

Figure A.8: Wave elevation and buoy response for waveform 8.

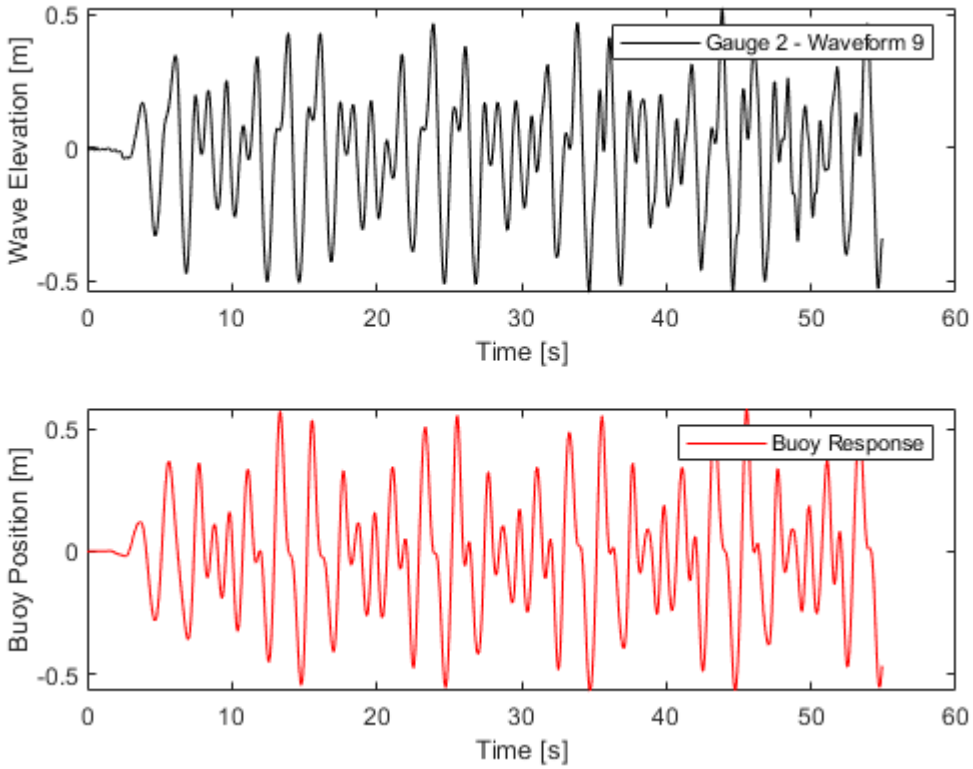

Figure A.9: Wave elevation and buoy response for waveform 9.

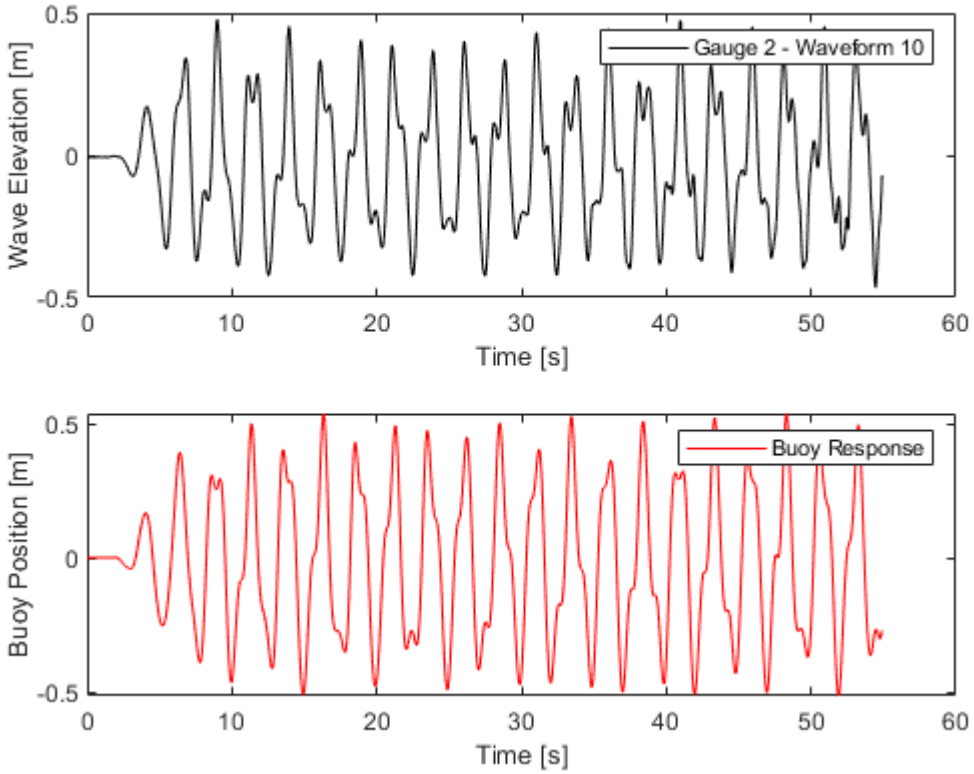

Figure A.10: Wave elevation and buoy response for waveform 10.

Appendix B

Gauge Position

For this study, the gauges were placed around the buoy and are described relative to the buoy. This means the buoy exists only at the origin (0,0). Figure B.1 demonstrates the coordinate system for this study. The x-direction is in the direction that the waves travel, and the y-direction is across the tank. The corresponding mathematical signs to these directions are displayed on the figure.

Displayed in Table B.1 are the specific coordinates for each wave gauge.

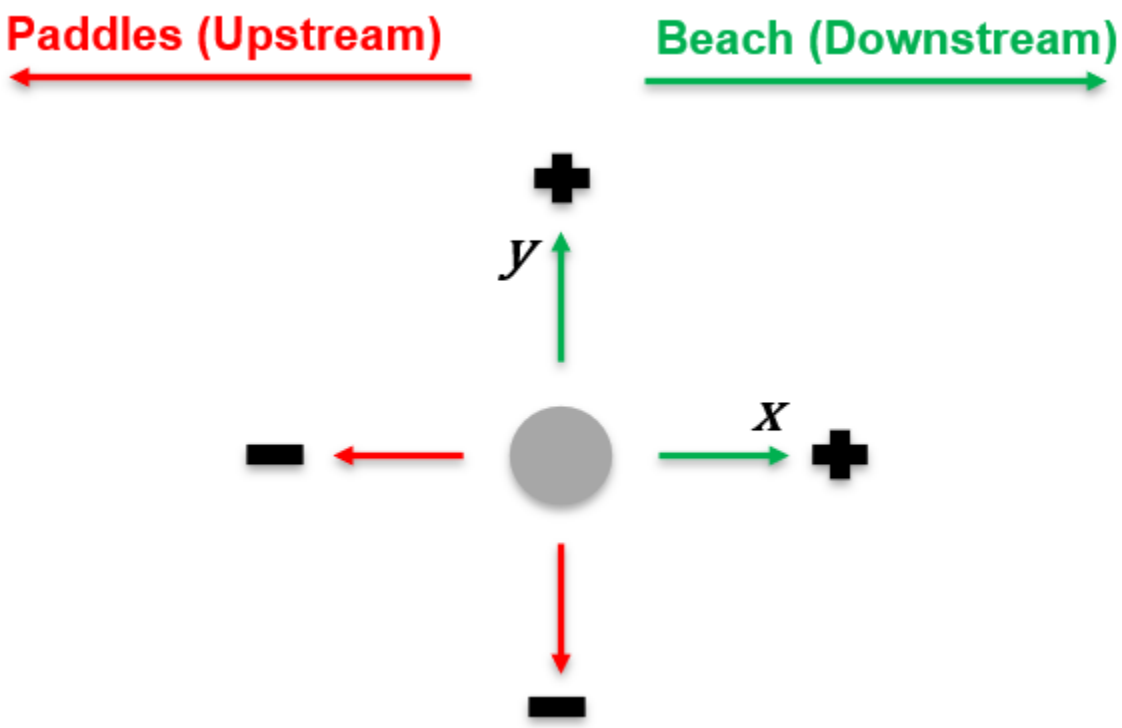

Figure B.1: Coordinate system relative to the buoy.

Table B.1
Gauge locations relative to the buoy at the origin (0,0).

#	x, m	y, m
1	-2.21	-0.86
2	-2.16	0.06
3	-2.11	0.97
4	-0.48	-0.91
5	-0.48	0.04
6	-0.48	0.96
7	0.75	-1.02
8	0.77	0.14
9	0.78	0.97
10	1.66	-1.03
11	1.68	0.02
12	1.70	1.00